Bulletin of Mathematical Biology (2004) **66**, 199–232
doi:10.1016/j.bulm.2003.06.001

A Computational Model of the Mechanics of Growth of the Villous Trophoblast Bilayer

KATARZYNA A. REJNIAK*
Mathematical Biosciences Institute,
The Ohio State University,
231 West 18th Avenue,
Columbus, OH 43210-1744,
USA
E-mail: rejniak@mbi.osu.edu

HARVEY J. KLIMAN
Department of Obstetrics, Gynecology and Reproductive Sciences,
Yale University School of Medicine,
New Haven, CT 06520,
USA

LISA J. FAUCI
Department of Mathematics,
Tulane University,
New Orleans, LA 70118,
USA

We present a computational model of the mechanics of growth of the trophoblast bilayer in a chorionic villous, the basic structure of the placenta. The placental trophoblast is modeled as a collection of elastic neutrally buoyant membranes (mononuclear cytotrophoblasts and multinucleated syncytiotrophoblast) filled with a viscous, incompressible fluid (cytoplasm) with sources of growth located inside cells. We show how this complex, dynamic fluid-based structure can be modeled successfully using the immersed boundary method. The results of our research presented here include simulations of two processes—cell proliferation and cell fusion which both play a crucial role in the growth and development of the trophoblast tissue. We present the computed results of simulations of both processes running independently as well as simultaneously, along with comparisons with clinically obtained results.

*Author to whom correspondence should be addressed.

0092-8240/04/020199 + 34 $30.00/0

1. INTRODUCTION

The trophoblast tissue is formed at a very early stage of pregnancy. The first appearance of the trophoblast cells takes place by the fourth day after fertilization. By 9 days of gestation the embryo is already surrounded by two layers of trophoblasts—the inner mononuclear *cytotrophoblasts* (CTs) and the outer multinucleated *syncytiotrophoblast* (ST). At about 3 weeks after fertilization, the first *chorionic villi* are formed, establishing the supporting structure of the fetal circulatory system. Each of the chorionic villi is covered by a thin layer of supportive matrix, called the basement membrane, and the two layers of trophoblasts. These three layers together separate the mesenchymal core of the villous (where the fetal capillaries are located) from the intervillous space filled with maternal blood. This organizational paradigm remains the basis of the structure and function of the placenta until delivery.

Although the basic structure of the placenta is established by 4 weeks of development, the placenta will grow extensively from less than 1 cm in diameter in the 4th week of gestation to approximately 22 cm in diameter at term. However, the relationship between the fetus and the mother will remain unchanged. Nutrients and oxygen dissolved in the mother's blood diffuse through the trophoblast layers and then into the bloodstream of the fetus and, likewise, waste products pass through the trophoblast layers from the blood of the fetus to that of the mother [cf. Benirschke and Kaufmann (1995), Boyd and Hamilton (1970), Kliman (1999) for more details]. A photomicrograph of a representative section of the straight portion of a chorionic villous is shown in Fig. 1.

1.1. ***The trophoblast.*** We present here a short description of the structure and functions of both layers of the trophoblast tissue. More details can be found in Benirschke and Kaufmann (1995), Boyd and Hamilton (1970), Kliman (1999), Kliman *et al*. (1986, 1987) and Mayhew (2001).

The syncytiotrophoblast layer constitutes a syncytium, i.e., it is made up of large masses of cytoplasm containing up to a hundred nuclei and extends over the surfaces of all villous trees. At the early stages of pregnancy this layer is homogeneous with evenly dispersed nuclei. At term the numerous nuclei are distributed irregularly and the outer surface of the ST layer, which is in direct contact with the mother's blood, is also irregular with protuberances called syncytial knots. The syncytiotrophoblastic nuclei are not capable of proliferation and therefore the ST layer can grow and regenerate only through cell fusion from the CT layer (Kliman *et al*., 1986).

The cytotrophoblast layer consists of large individual cells with diameters of 10 μm on average, but occasionally up to 20–30 μm. Single cells are of an irregular ovoid shape, but arranged as a layer, they are oval or cuboidal. In general, the CT is undifferentiated or poorly differentiated when compared with the ST. The CT cells are, however, capable of continuous proliferation and recruitment by fusion into

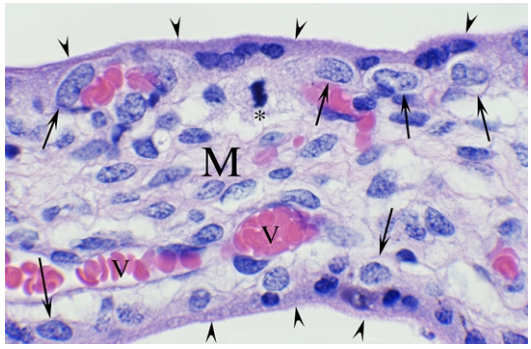

Figure 1. Straight portion of a representative chorionic villous. The villous is covered by a bilayer of trophoblasts consisting of the inner proliferative CTs (arrows) and the overlying ST (arrow heads). Vessels (V) containing fetal erythrocytes can be seen within the supporting mesenchymal core (M). The proliferative nature of the CTs is confirmed by the CT that is at the metaphase stage of mitosis ($*$).

the ST layer. At the early stages of pregnancy the CT layer is continuous. Later on however, the CT cells become widely separated. This is due to the fact that at the later stages of pregnancy, the growth, branching and expansion of the surface of chorionic villi are so rapid that the CT cells become widely spread below the ST layer, even as the total number of CT cells increases steadily until term.

1.2. ***Description of the clinical problem motivating our research.*** Results of clinical research establish the connection of appearances of trophoblast invaginations (deep inward tissue bending) in the placenta with pregnancy losses and complications. It was shown (Honore *et al*., 1976; Novak *et al*., 1988; Silvestre *et al*., 1996; Lewis and Perrin, 1999; Kliman *et al*., 2001; Kliman and French, 2001; Kliman and Segel, 2003) that the normally regular and smooth covering formed by layers of the trophoblast tissue can be disturbed, leading to trophoblast invaginations, inclusions and tissue scalloping. These invaginations appear very rarely in normal, healthy placentas (less than 3% of placentas from uncomplicated, normal gestations), but were found very often in the placentas of fetuses with known chromosomal abnormalities (93% of examined cases). Because the only cell processes which cause growth and development of the trophoblast tissue are cell proliferation and cell fusion, we have analyzed how the interaction of these two processes, as well as space and time distribution of fusing and proliferating cells, may result in such tissue bending.

2. THE MATHEMATICAL MODEL

The formulation of our computational model is based on the immersed boundary method, first introduced by Peskin for the study of flow patterns around heart valves in Peskin (1972). This method for capturing fluid–structure interactions couples

the elastic forces generated by immersed structures with a surrounding viscous, incompressible fluid. The immersed, elastic structures may be thought of as δ-function layers that exert force on the fluid, but at the same time move at the local fluid velocity. The immersed boundary method has been successfully applied to the problems in biological fluid dynamics, including blood flow in the heart (Peskin, 1977; McQueen and Peskin, 1989; Peskin and McQueen, 1989), valveless pumping (Jung and Peskin, 2001), arteriolar flow (Arthurs *et al*., 1998), platelet aggregation during blood clotting (Fogelson, 1984; Fauci and Fogelson, 1993), motion of cilia, flagella and aquatic animals (Fauci and Peskin, 1988; Fauci, 1990; Dillon *et al*., 1995; Dillon and Fauci, 2000b, 2001), biofilm processes and swimming of multiple microorganisms (Dillon *et al*., 1996; Dillon and Fauci, 2000a), locomotion and deformation of ameboid cells (Bottino and Fauci, 1998; Bottino, 1998), outgrowth of the vertebrate limb bud (Dillon and Othmer, 1999). The power of the immersed boundary method is that it can handle very complicated geometries, as well as the interaction of multiple immersed boundaries.

In this model of trophoblast tissue, our immersed boundaries are the cell membranes. The surrounding fluid, both inside and outside of the cells, is assumed to be of the same viscosity and density. In addition, cell growth is modeled by tracking fluid sources located at the nuclei of the cells. We begin with a model of a linear segment of the chorionic villous. Periodic boundary conditions for the fluid are imposed on the domain. The motivation for using such a model is to focus upon the behavior of a single cell or a small group of cells. Our model consists of three main elements: a basement membrane, a layer of several cytotrophoblastic cells and a layer of syncytium. Initially, all CT cells have rectangular shapes and their nuclei are located in the geometrical center of each cell. The ST layer is modeled as a wide, initially horizontal, strip with several nuclei evenly distributed inside it. We adopt a simplified assumption that the mesenchymal matrix enclosed by the basement membrane, the cytoplasm inside the trophoblast, and the mother's blood outside the layer of syncytium are composed of a Newtonian fluid of the same density and viscosity. However, additional elastic forces are superimposed to capture the viscoelastic nature of the cytoplasm. The corresponding geometrical representation of this computational model is shown in Fig. 2.

The boundaries of the ST layer, the membranes of the CT cells and the basement membrane are all modeled as thin elastic neutrally buoyant bands. This is accomplished by connecting adjacent boundary points with linear springs. The viscoelastic nature of the cytoplasm in both layers is modeled by additional linear springs that attach opposite points on the CT cell membranes and opposite points on the membranes of the ST layer respectively. The structure of a portion of the trophoblast showing the CT cells and the ST layer is presented in Fig. 3.

2.1. ***Mathematical framework.*** The philosophy behind the immersed boundary method is that the fluid is influenced by forces generated by the immersed, elastic boundaries, as well as by sinks and sources of fluid distributed in the fluid domain.

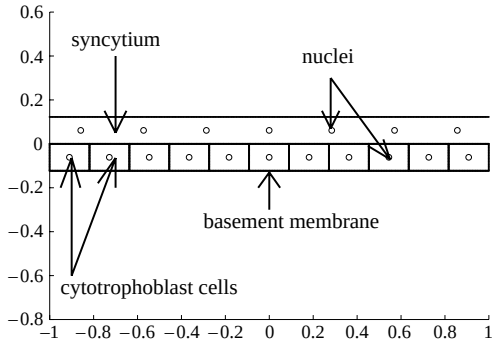

Figure 2. A two-dimensional model of the structure of the trophoblast tissue. The inner (lower) layer consists of several individual mononuclear cytotrophoblastic cells. The outer (upper) layer is the syncytium, a continuous mass of cytoplasm with numerous nuclei located inside it (circles). In this configuration, the lower line of the CT cells coincides with the basement membrane. The upper line of the CT cells coincides with the lower boundary of the ST layer. The tissue is immersed in a viscous, incompressible fluid.

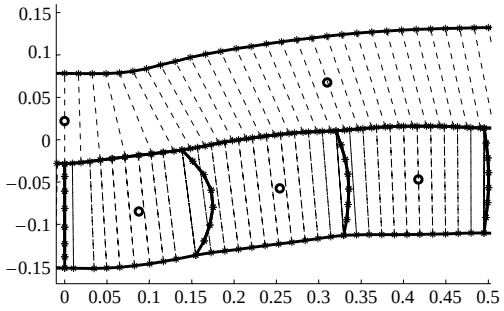

Figure 3. A two-dimensional model of the structure of the CT cells and the ST layer. The elastic membrane of each cell is shown as boundary points (stars) connected by linear springs (solid thick lines). Nuclei (circles) are located inside cells. The cytoskeleton is represented by linear springs (dashed thin lines) between opposite boundary points.

The motion of such fluid is governed by the Navier–Stokes equations (Batchelor, 1967; Peskin, 1977):

$$\rho\frac{\partial \mathbf{u}}{\partial t} + \rho(\mathbf{u}\cdot\nabla)\mathbf{u} = -\nabla p + \mu\Delta\mathbf{u} + \frac{\mu}{3\rho}\nabla s + \mathbf{f} \tag{1}$$

$$\rho\nabla\cdot\mathbf{u} = s. \tag{2}$$

Equation (1) is Newton's second law. Here, $\mathbf{u} = (u, v)$ is local fluid velocity, ρ is fluid density, μ is the fluid viscosity, p is pressure, s is the local fluid expansion, and $\mathbf{f}$ is the force due to the immersed boundaries.

Equation (2) is the law of mass conservation. The fluid in our model is assumed to be incompressible, except at a discrete collection of isolated point sources and sinks that we use to model the growth and fusion of cells. Therefore the source

distribution s (and the local rate of expansion of the velocity field $\nabla \cdot \mathbf{u}$) is not identically equal to zero on the whole fluid domain. However, it is nonzero only at these isolated points. In order to satisfy conservation of mass globally on the fluid domain, we require that the total balance of source and sink distributions be equal to zero at every time t, i.e., $\int_\Omega s(\mathbf{x}, t)d\mathbf{x} = \rho \int_\Omega (\nabla \cdot \mathbf{u})d\mathbf{x} = 0$. Therefore, in the situation when sources and sinks located in the tissue nuclei do not balance each other, we must create a series of artificial sinks (or sources) of small strength, which are located sufficiently far from the tissue so as not to influence its motion.

The boundaries of the trophoblast tissue at time t are represented by $\mathbf{X}(l, t)$ where l is a Lagrangian parameter such as arclength. $\mathbf{Y}_k(t)$ represents coordinates of trophoblastic nuclei.

The force density $\mathbf{f}$ in equation (1) captures the forces $\mathbf{F}$ generated by the elastic, immersed boundaries. These forces are spread in the δ-layer region of fluid which coincides with material points Γ of their boundaries:

$$\mathbf{f}(\mathbf{x}, t) = \int_\Gamma \mathbf{F}(l, t)\delta(\mathbf{x} - \mathbf{X}(l, t))dl \tag{3}$$

here δ is the two-dimensional Dirac delta function. $\mathbf{X}(l, t)$ represents coordinates of the material points of the immersed boundaries of the trophoblast bilayer. Away from these material points, the force density on the fluid is zero.

In our model, we deal with several elastic boundaries immersed in the cytoplasm: the basement membrane, the CT cells and the layer of syncytium. Every boundary point $\mathbf{X}_k$ of each of these tissue components is connected to its two neighbors $\mathbf{X}_{k-1}$ and $\mathbf{X}_{k+1}$ by linear, elastic springs. The forces due to these springs are of the form:

$$\mathbf{F}_k^{\text{adj}} = \sum_{p=k-1,\, p\neq k}^{k+1} \mathcal{S}_{\text{adj}} \frac{\|\mathbf{X}_k - \mathbf{X}_p\| - \mathcal{L}_{\text{adj}}}{\|\mathbf{X}_k - \mathbf{X}_p\|}(\mathbf{X}_k - \mathbf{X}_p) \tag{4}$$

where $\mathcal{S}_{\text{adj}}$ is a spring stiffness constant and $\mathcal{L}_{\text{adj}}$ is the resting length. The initial spacing between adjacent pairs of immersed boundary points is also given by the resting length $\mathcal{L}_{\text{adj}}$.

Moreover, every point $\mathbf{X}_k$ on the lower and upper boundaries of each CT cell and on the lower and upper boundaries of the ST layer is also connected to the corresponding opposite point $\mathbf{X}'_k$ by an additional force of the form (the opposite forces):

$$\mathbf{F}_k^{\text{opp}} = \mathcal{S}_{\text{opp}} \frac{\|\mathbf{X}_k - \mathbf{X}'_k\| - \mathcal{L}_{\text{opp}}}{\|\mathbf{X}_k - \mathbf{X}'_k\|}(\mathbf{X}_k - \mathbf{X}'_k) \tag{5}$$

where $\mathcal{S}_{\text{opp}}$ is a spring stiffness constant and $\mathcal{L}_{\text{opp}}$ is the resting length. The initial spacing between opposite pairs of immersed boundary points is also given by the resting length $\mathcal{L}_{\text{opp}}$ and is equal to the nominal cell width.

The total elastic force at each immersed boundary point is the sum of the adjacent and opposite spring forces, $\mathbf{F}_k = \mathbf{F}_k^{\text{adj}} + \mathbf{F}_k^{\text{opp}}$. The stiffness constant for each

kind of connection (adjacent and opposite) and for each of the three tissue components (the basement membrane, the ST layer and the cytotrophoblastic cells) may be chosen differently in our model. All adjacent springs and opposite connections are preserved during the whole process of tissue development. This includes instances when boundary points are removed or added, causing some connections to be rearranged.

Similarly, sources of fluid S are spread only locally in the δ-layer region of fluid which coincides with material points Ξ, where sources ($S > 0$) and sinks ($S < 0$) are defined:

$$s(\mathbf{x}, t) = \sum_{k \in \Xi} S_k(t)\delta(\mathbf{x} - \mathbf{Y}_k(t)) \tag{6}$$

here δ is the two-dimensional Dirac delta function. $\mathbf{Y}_k(t)$ represents coordinates of the material points of tissue nuclei. Away from these material points, the source distribution on the fluid is zero.

The material points of immersed boundaries $\mathbf{X}(l, t)$ and tissue nuclei $\mathbf{Y}_k(t)$ are then moved at the local fluid velocity:

$$\frac{\partial \mathbf{X}}{\partial t} = \mathbf{u}(\mathbf{X}(l, t), t) = \int_{\Omega} \mathbf{u}(\mathbf{x})\delta(\mathbf{x} - \mathbf{X}(l, t))d\mathbf{x}. \tag{7}$$

2.2. ***Numerical implementation.*** We choose a finite difference, regular, rectangular grid to represent the fluid domain. In addition, the cell membranes $\mathbf{X}(l, t)$ are discretized and represented as immersed boundary points or nodes $\mathbf{X}_k(t)$. The most important part of the immersed boundary method is the way in which the interaction between these two structures—fluid and elastic objects embedded in it—is modeled. A discretized Dirac delta function plays a crucial role in such modeling. It defines how the velocity field is interpolated from the fluid grid to the immersed boundary points, and how the forces are spread from the boundary points to the nearby grid points. Moreover, the sinks and sources of fluid that are defined at the isolated points (the trophoblast nuclei) must influence the fluid grid using a discretized Dirac delta function. There are various possible choices of discretized delta function [e.g., Peskin (1972, 1977, 2002), Peskin and McQueen (1995), Cortez and Minion (2000)]. We use the following function: $\mathcal{D}(\mathbf{x}) = d_h(x) \cdot d_h(y)$, where h is the grid spacing and:

$$d_h(r) = \begin{cases} \frac{1+\cos\left(\frac{\pi r}{2h}\right)}{4h} & \text{if } |r| < 2h \\ 0 & \text{if } |r| \geq 2h. \end{cases} \tag{8}$$

To illustrate the way in which the discrete delta function $\mathcal{D}$ handles interaction between material points and the fluid grid, we present three cases when it is applied in our tissue model. All figures show the situation when one of the cytotrophoblastic cells has proliferated and their two daughter cells are growing.

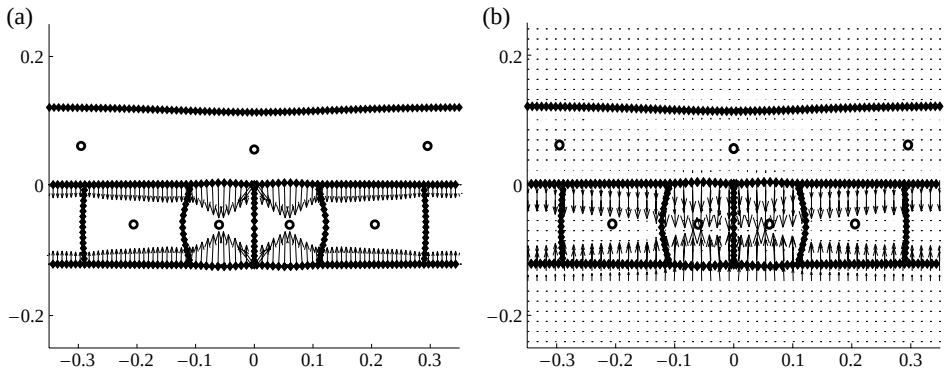

Figure 4. The forces defined on the immersed boundaries (frame 4a) are spread to the fluid grid in the thin δ-layer around the material points (frame 4b).

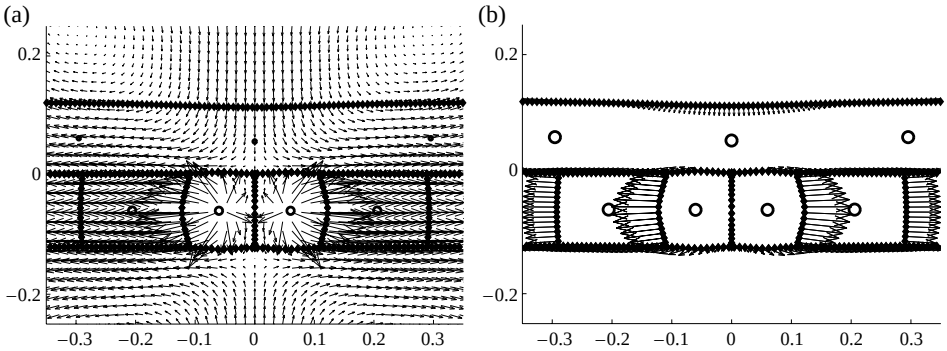

Figure 5. The velocity field defined at the fluid grid (frame 5a) is interpolated to the material points of the immersed boundaries in the thin δ-layer around the material points (frame 5b).

The growing cells cause the movement of the immersed boundary points of the cell membrane. Once the distance between adjacent or opposite points differs from their resting length, the corresponding adjacent or opposite forces are generated [Fig. 4(a)]. These boundary forces are then spread to the neighboring fluid grid [Fig. 4(b)]. Note that the spreading takes place only inside the thin δ-layer.

Similarly, the velocity field defined on the fluid grid [Fig. 5(a)] is interpolated to the material points of the immersed boundaries [Fig. 5(b)]. Note that the velocities of material points are influenced only by the fluid field inside the thin δ-layer around the boundary points.

Figure 6(a) shows the support of the discrete approximation $\mathcal{D}$ of the Dirac delta function which consists of 16 fluid grid points that receive a contribution from the source spreading. The corresponding source distribution is plotted in Fig. 6(b).

2.3. ***Discretization of fluid equations.*** In order to implement the method described above, we discretize the square fluid domain $\Omega = [-L, L] \times [-L, L]$ as an

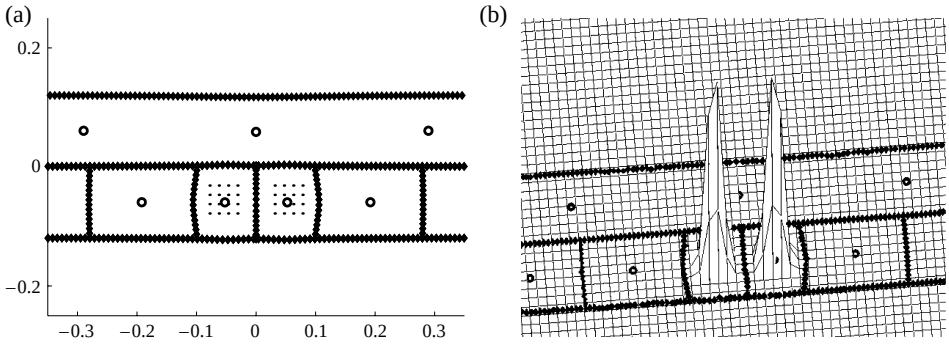

Figure 6. The 16-point source support consists of the fluid grid points (dots) near the cell center (circle) which receive a contribution from the source spreading (frame 6a). The corresponding source distribution is plotted (frame 6b).

$N \times N$ uniform square grid with mesh width $h = 2L/N$. The Navier–Stokes equations (1) and (2) are discretized as follows:

$$\begin{cases} \rho\left(\frac{u_r^{n+1}-u_r^n}{\Delta t} + \sum_{s=1}^{2} u_s^n D_s^{\pm} u_r^n\right) &= -D_r^0 p^{n+1} + \mu \sum_{s=1}^{2} D_s^+ D_s^- u_r^{n+1} \\ & \quad + \frac{\mu}{3\rho} D_r^o s^n + f_r^n \\ \rho \sum_{s=1}^{2} D_s^0 u_s^{n+1} &= s^n \end{cases} \tag{9}$$

where $r = 1, 2$ denotes respectively first or second vector field component, D_s^+ is the forward difference, D_s^- is the backward difference, D_s^0 is the center difference and $D_s^{\pm}$ is the upwind divided difference operator. This system of difference equations is solved for the unknown velocity field $\mathbf{u}^{n+1}$ by applying the discrete Fourier transformation (Dillon and Othmer, 1999).

The difference scheme (9) is stable provided that $\|\mathbf{u}^n\| \Delta t \leq h$. This CFL stability condition is necessary because of the fully explicit scheme used for the hyperbolic part of the Navier–Stokes equations. Moreover, the scheme is first order in space due to the upwind discretization of the term $(\mathbf{u} \cdot \nabla)\mathbf{u}$. It is also first order in time.

The numerical algorithm for the immersed boundary method can be summarized as follows. At the end of time step n we are given values of the fluid velocity field $\mathbf{u}^n$ on the square grid, the configuration of the immersed boundary points $\mathbf{X}_k^n$ on cell membranes, and positions of cell nuclei $\mathbf{Y}_l^n$. These values are updated at the next time step in the following way:

(1) Determine the source distribution S^n at the nuclei of growing or fusing cells, in the nuclei inside syncytium and in the lower and upper boundaries of the fluid domain.
(2) Spread the source distribution to the neighboring grid points to determine the local growth rate s^n of the fluid.
(3) Calculate the force density $\mathbf{F}^n$ from the cell membranes configuration $\mathbf{X}_k^n$ by computing the spring forces between adjacent and opposite boundary points.

Table 1. Numerical values of computational parameters.

Physical quantity	Computational parameter
Grid size	$N = 256$
Grid mesh	$h = 7.8125\ \mu$m
Time step	$\Delta t = 0.01$ s
Material points separation	$h_b = h/2$
Fluid viscosity	$\mu = 0.01$ g cm^{-1} s^{-1}
Fluid density	$\rho = 1$ g cm^{-3}
Source strength	$S_0 = 10^{-6}$ g s^{-1}
Resting length of adjacent springs	$\mathcal{L}_{\text{adj}} = h_b$
Resting length of opposite springs	$\mathcal{L}_{\text{opp}} = 120\ \mu$m
Spring stiffness of adjacent (*adj*) and opposite (*opp*) connections:	
in the CT cells	$\mathcal{S}^{\text{CT}}_{\text{adj}} = \mathcal{S}^{\text{CT}}_{\text{opp}} = \mathcal{S} = 0.1$ g s^{-2}
in the ST layer	$\mathcal{S}^{ST}_{\text{adj}} = \mathcal{S}^{\text{ST}}_{\text{opp}} = \mathcal{S}/25$
in the basement membrane	$\mathcal{S}^{BM}_{\text{adj}} = 10 \cdot \mathcal{S}$

(4) Spread the force densities to the neighboring grid points to determine the forces $\mathbf{f}^n$ on the fluid.
(5) Solve the Navier–Stokes equations for the fluid velocities $\mathbf{u}^{n+1}$ by using the fast Fourier algorithm.
(6) Interpolate the fluid velocity field $\mathbf{u}^{n+1}$ to each immersed boundary point on cell membranes and to each nuclei in the CT cells and syncytium.
(7) Compute new positions of the boundary points $\mathbf{X}_k^{n+1}$ and new positions of the nuclei $\mathbf{Y}_l^{n+1}$ by moving them at the local fluid velocity using a forward Euler step.

More details about an implementation of this algorithm, in particular the numerical solution of the Navier–Stokes equations, can be found in Dillon and Othmer (1999) or Rejniak (2002).

In each simulation presented below, the fluid domain is represented by a 256×256 finite-difference grid. The tissue consists initially of 11 equal rectangular CT cells, a horizontal layer of syncytium, and a horizontal line of basement membrane. The basement membrane is the most rigid among the three tissue components, whereas the layer of syncytium is the most flexible. These differences in elastic properties are achieved by appropriate choices of stiffness constants. The resting lengths of all adjacent springs in the basement membrane, CT and ST layers are set equal to the initial separation of the boundary points. The resting lengths of all opposite springs in the CT and ST layers are set equal to the initial cell height. All sources and sinks defined at the cell nuclei have the same strength. In case they do not balance each other (as may take place during cell growth), a collection of small artificial sinks is created along the upper and lower boundaries of the fluid domain. The numerical values of all computational parameters are presented in Table 1.

The Reynolds number $Re = \rho LU/\mu$ governing the fluid dynamics of trophoblast growth is of order 10^{-9}. A characteristic length-scale is equal to the diameter of

a large cytotrophoblastic cell, $L = 20\ \mu$m. A characteristic velocity is computed based on the laboratory experiment of two CTs migrating toward each other on the distance of 30 μm in 24 h, as presented in Kliman *et al*. (1987). We use the numerical Reynolds number equal to 5.9×10^{-5}. A characteristic length-scale is chosen to be equal to 200 μm and the characteristic velocity scale is equal to the average cytoplasmic velocity during the cell growth, $U = 3.28 \times 10^{-5}$ cm s^{-1}. These values do not faithfully represent the physical length and time scales of the trophoblast tissue. However, our goal is to build a computationally plausible model which approximates real tissue geometry and reflects the phenomena observed experimentally. In any case, the computations do faithfully represent the low Reynolds number regime of the physiological process. The computational time needed to complete the processes of cell fusion and cell proliferation are much shorter than in reality, but we have preserved the ratio between the timings of these two processes. The process of cell fusion takes 1.5–2 times longer than the process of cell proliferation. This is in agreement with the experimental results. The usual cell cycle, including cell division and cell growth, lasts about 24 h. The cultured CTs undergo cell aggregation and fusion between 24 and 72 h of culture (Kliman *et al*., 1986, 1987).

3. Numerical Simulations of Cell Processes

The cytotrophoblastic cells can undergo two kinds of processes—cell proliferation and cell fusion which both influence development of the whole trophoblast tissue. In this section we discuss how these processes are modeled in our study. We also present computer simulations showing the effect of proliferation (Section 3.1) or fusion (Section 3.2) of a single CT cell on the shape of the trophoblast tissue.

3.1. ***Modeling proliferation.*** The process of cell proliferation in our computational model comprises events occurring on the cellular level only and consists of two stages. First the large mother cell is divided into two smaller cells (cytokinesis) which is modeled as a one-step process by introducing a new boundary, which splits the mother cell into two smaller daughter cells of approximately equal areas. After division of the mother cell is completed, we create two new nuclei and two sources of growth, both located at the centers of each daughter cell and initiate the second stage of proliferation—cell growth. This process is modeled as a long event (a few hundreds of time steps), in which sources located at cell centers increase the amount of fluid inside each cell and cause cell growth by moving their boundaries apart from the sources. The area of growing cells is monitored and sources are inactivated once the cells reach the size of their mother cell. Figure 7 shows several snapshots of the fluid velocity field and the trophoblast tissue immersed in it during the proliferation of a single cell located in the middle of the CT.

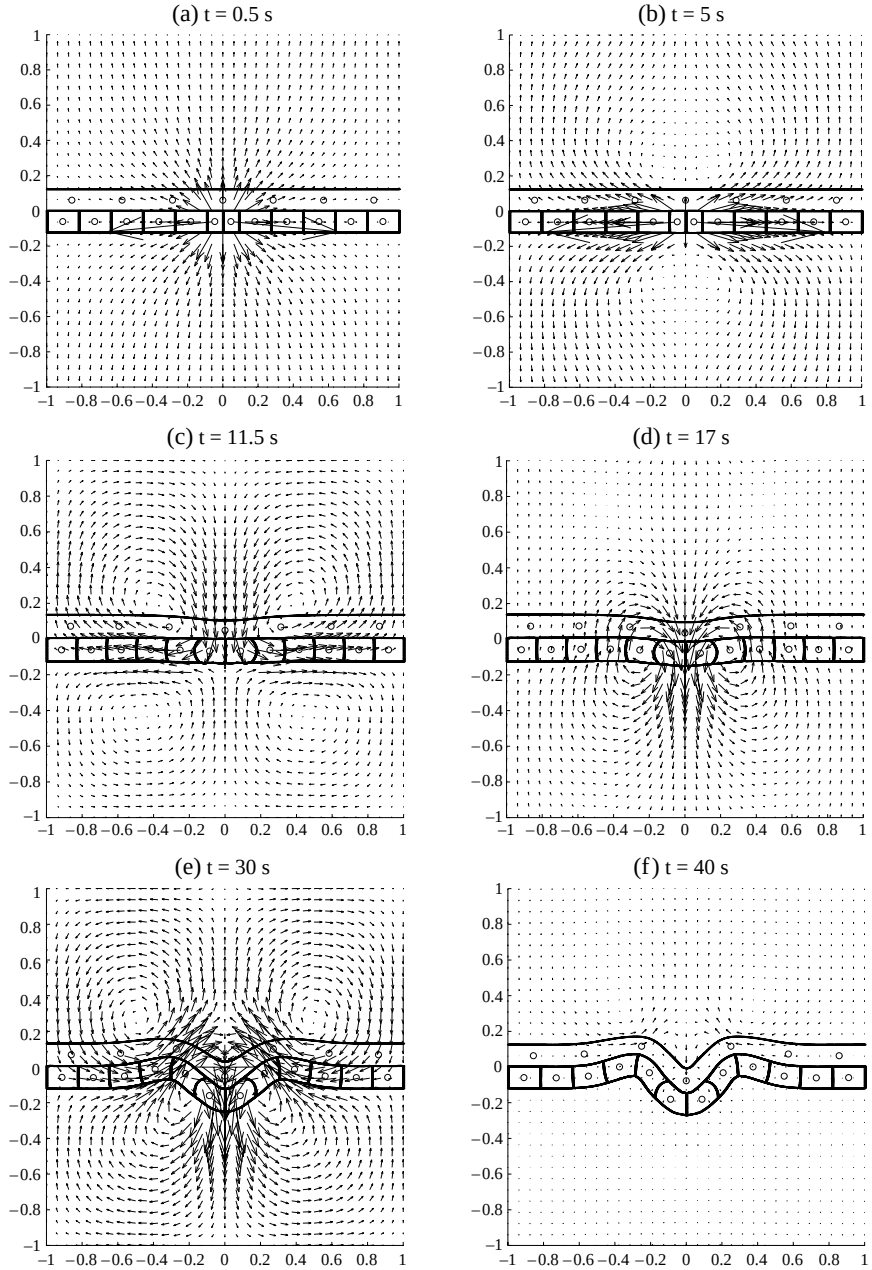

Figure 7. Simulation of the development of the trophoblast tissue during proliferation of a single CT cell. This simulation starts with the division of the mother cell into two daughter cells (frame 7a), includes cell growth, which is accomplished when both daughter cells double their size (frame 7c), and is finished when the tissue shape stabilizes and the fluid field vanishes(frame 7f).

It is a simplification of the model that the source of growth is placed at the cell's center. Biological cells do get the fluid required for growth through their

cell membranes. However, we are not trying to capture this level of detail in our model of trophoblast bilayer.

The source strength in our model is adjusted to obtain a desired velocity of cytoplasm during the cell growth. Changing the source strength will affect time needed to complete the processes of cell fusion and cell proliferation, but will not change the final tissue configuration.

3.2. ***Modeling fusion.*** Our goal here is to model fusion from the CT layer into the syncytium by moving the nucleus and the cytoplasm from the fusing cell into the layer of ST. This can be viewed as aggregation of the CT cell and syncytium. The way we have chosen to model this process is to introduce a sink inside the fusing cell and a source in the ST layer which together cause the fluid to move from the inner to the outer layer. This is a rather long event (about 1500 time steps). The area of the fusing cell is monitored and the source and the sink are both inactivated once the fusing cell reaches the prescribed 'zero' area. All boundary points and opposite connections of the fusing cell must be rearranged and finally removed during this process, which corresponds to membrane disintegration. Figure 8 shows several snapshots of the fluid velocity field and the trophoblast tissue immersed in it during fusion of a single cell located in the middle of the CT.

4. Simulations of Tissue Bending

In this section we present several illustrative numerical simulations in which the initially horizontal trophoblast tissue is exposed to different cell processes. These simulations show how the development of the trophoblast tissue and its final shape depend not only on the type of cell processes, but also on their spatial and temporal distributions (Sections 4.1 and 4.2). We also discuss in this section how the initiation of cell processes causes the inward or outward tissue bending (Section 4.3) and tissue invaginations (Section 4.4). In each numerical experiment presented here the trophoblast tissue has a horizontal configuration initially and the simulation is completed when the shape of the tissue stabilizes again.

4.1. ***Dependence on the order of cell processes.*** Two computer simulations presented in this section illustrate the difference in the development of the trophoblast tissue when the same cell processes are executed in the opposite order. We consider here a case when one cell fusion is accompanied by two simultaneous cell proliferations.

Figure 9 shows a sequence from a simulation in which the process of fusion precedes proliferations. Here we first fuse a cell located in the middle of the CT layer. After the process of cell fusion is completed we simultaneously divide two neighboring middle cells located symmetrically around the tissue center. Their growth causes the whole tissue to bend outward.

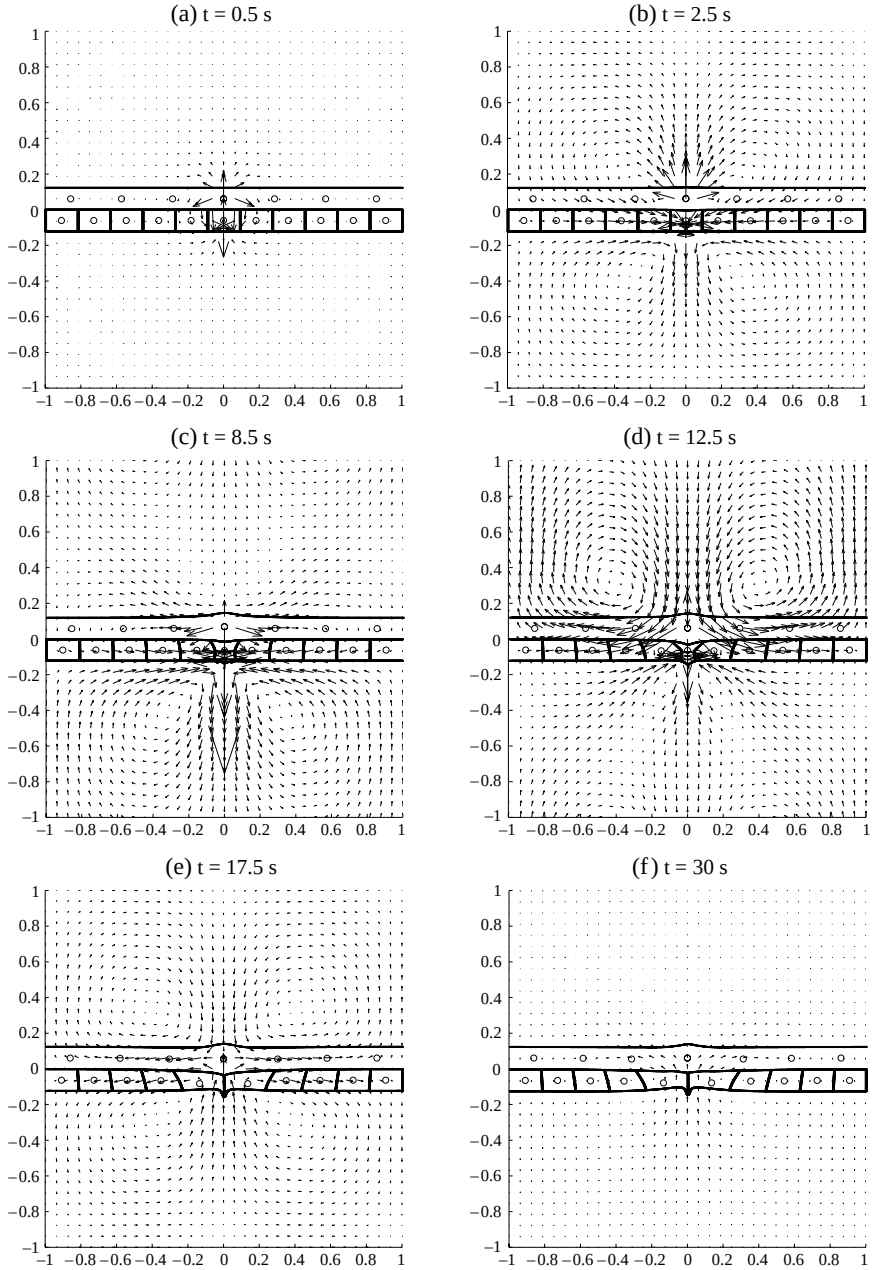

Figure 8. Simulation of the development of the trophoblast tissue during fusion of a single CT cell. This simulation starts with activation of a fluid source-sink pair (frame 8a) and is finished when the tissue shape stabilizes and the fluid field vanishes (frame 8f).

In the second simulation presented here the same cell processes are performed in the opposite order. First we simultaneously proliferate two cells located symmetrically around the middle cell in the CT layer. We allow all daughter cells to

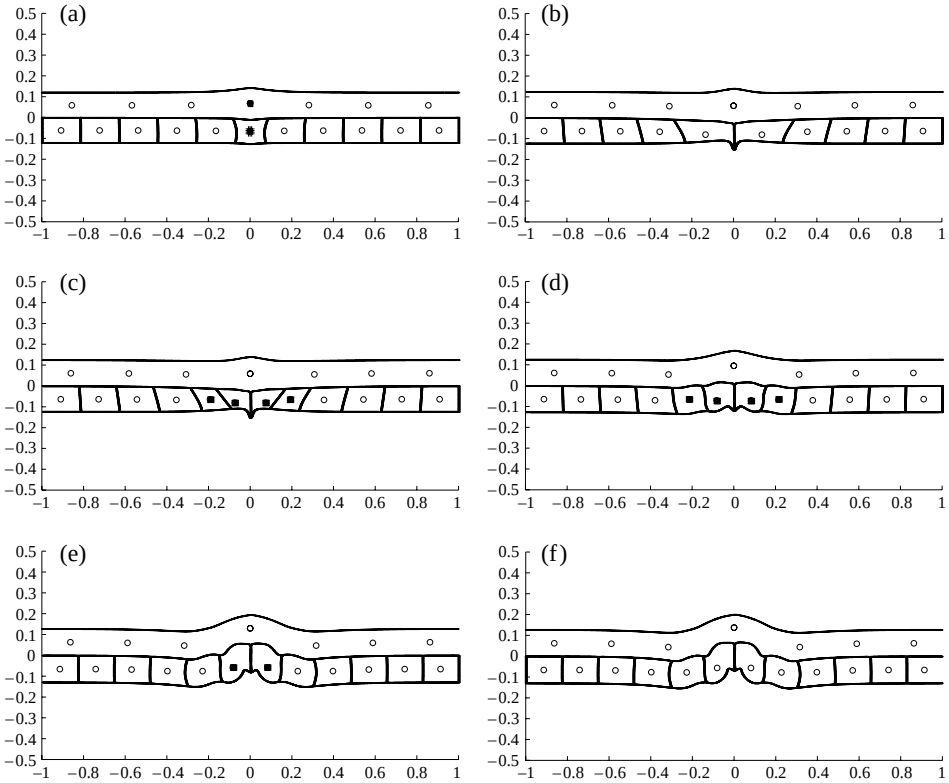

Figure 9. Simulation of the development of the trophoblast tissue during fusion of a single cell followed by two simultaneous cell proliferations; shown at times (a) $t = 6$ s; (b) $t = 21.5$ s; (c) $t = 22$ s; (d) $t = 27.5$ s; (e) $t = 31.5$ s; (f) $t = 32.5$ s. Black squares at cell nuclei indicate which cells are currently fusing or proliferating.

grow to the size of their mother cells and after the processes of cell growth are completed we fuse a cell in between. This order of cell processes results in the scalloping of the whole trophoblast tissue. Figure 10 shows several snapshots from this simulation.

These two numerical experiments show that the shape of the developing trophoblast tissue in our computational model depends not only on the kind and number of processes operating on the CT cells, but also on the order in which they are executed.

The case considered here (one cell fusion accompanied by two cell proliferations) states the condition which guarantees a regular flat shape of the trophoblast tissue with no bending in previous mathematical models discussed in Kliman *et al*. (2001). In our simulations the final tissue shape displays the effect of bending or scalloping, even if the number of cells in the CT and amount of cytoplasm in the syncytium are the same at the end of each experiment. These different results follow from the fact that the mathematical models introduced in Kliman *et al*. (2001), based on the relation between frequencies of observed processes of

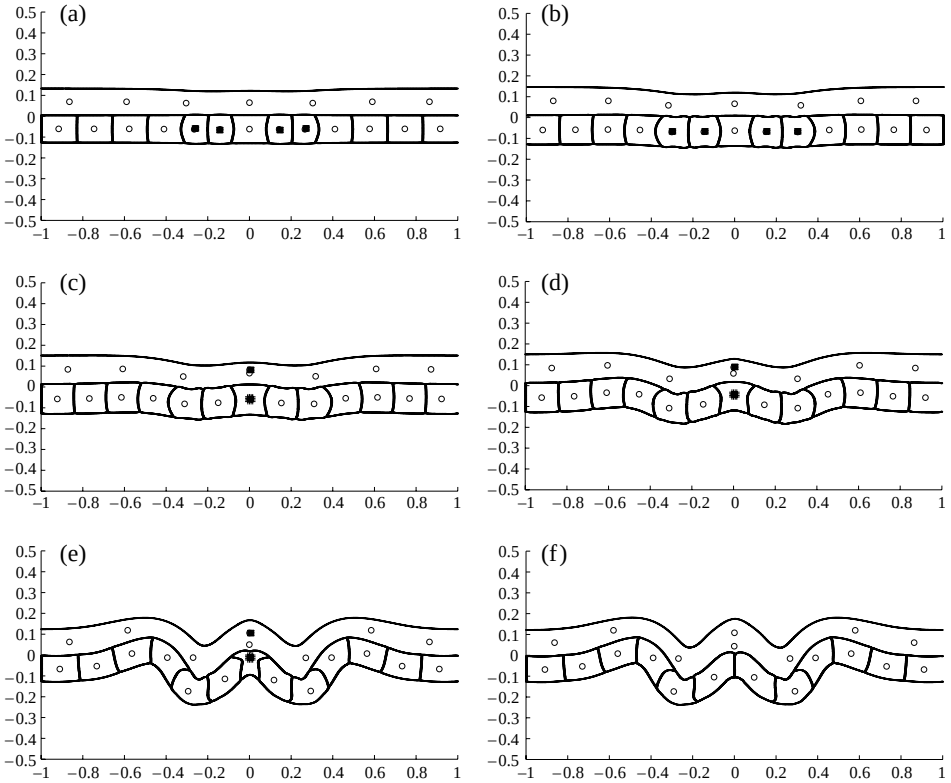

Figure 10. Simulation of the development of the trophoblast tissue during two simultaneous cell proliferations followed by a single cell fusion; shown at times (a) $t = 6$ s; (b) $t = 11$ s; (c) $t = 13$ s; (d) $t = 15$ s; (e) $t = 22.5$ s; (f) $t = 25.5$ s. Black squares at cell nuclei indicate which cells are currently fusing or proliferating.

cytotrophoblastic proliferation and fusion, assume that the cytoplasm distributions in both layers of the trophoblast are uniform. In contrast, we allow variable width of the ST during the tissue development. Moreover we take into account the elastic mechanics of the cells in a fluid medium.

4.2. ***Dependence of the spatial and temporal distribution of cell processes.*** We present here a computer simulation of a few processes (cell proliferations mixed with cell fusions) operating on the same tissue. All these processes together lead to a regular horizontal shape of the tissue without any pronounced inward or outward bending (Fig. 11). We compare this simulation with Figs. 7 and 12 and show that the different spatial and temporal distributions of cell processes result in the different shape of the trophoblast tissue. Moreover, the simulation presented in this section shows that the tissue bending is not an intrinsic feature of our model and that we are able to capture development that results in a regular tissue shape.

Figure 11 shows a sequence from a simulation in which one cell proliferation is followed by two simultaneous cell fusions and then again by one cell proliferation.

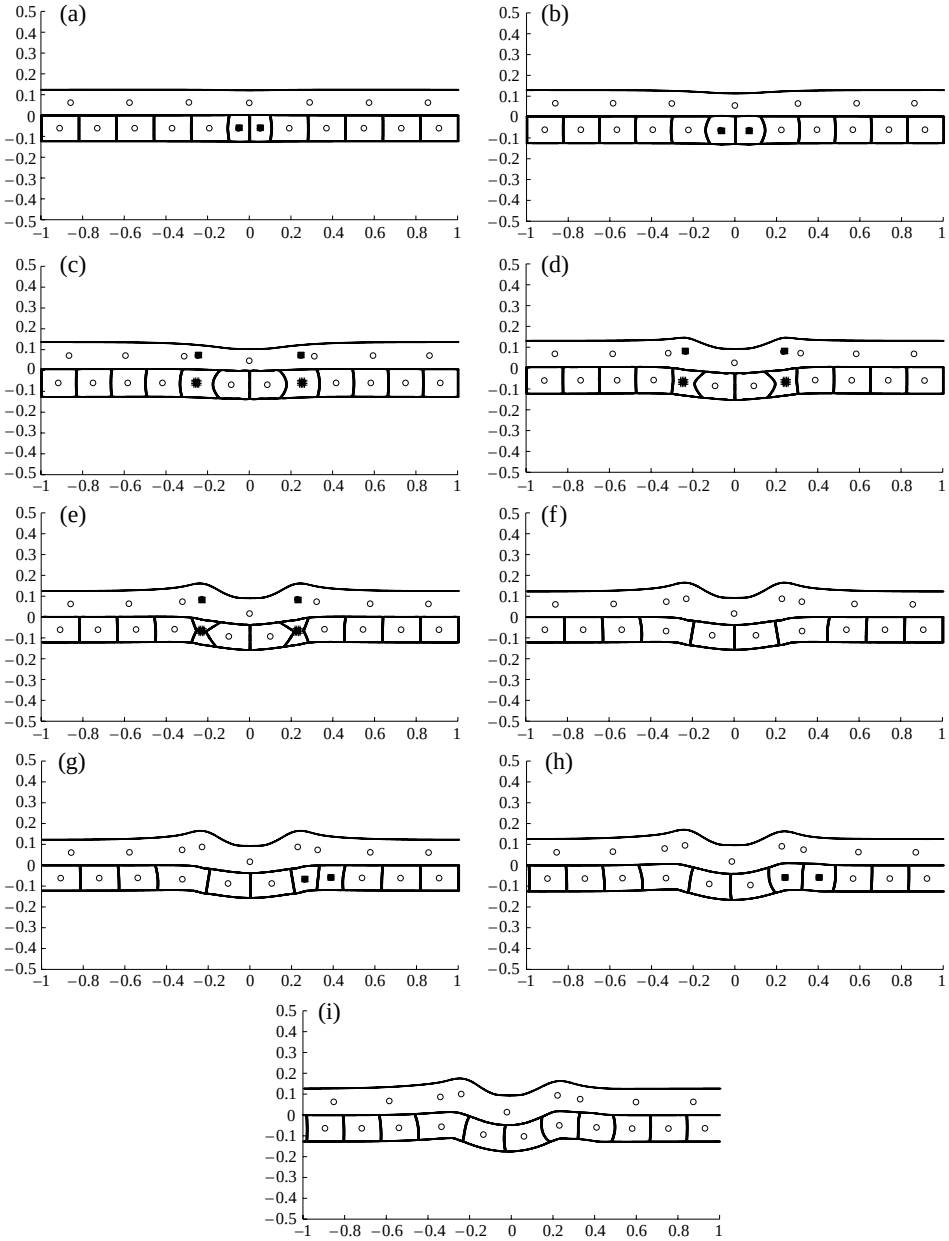

Figure 11. Simulation of the development of the trophoblast tissue during proliferation of a single cell followed by two simultaneous fusions of symmetrically located cells and by one more proliferation; shown at times (a) $t = 2.5$ s; (b) $t = 7.5$ s; (c) $t = 13$ s; (d) $t = 20$ s; (e) $t = 25$ s; (f) $t = 26.5$ s; (g) $t = 27$ s; (h) $t = 32.5$ s; (i) $t = 35$ s. Black squares at cell nuclei indicate which cells are currently fusing or proliferating.

At the beginning we divide a cell located at the middle of the CT layer and let its daughter cells reach maturity. Next we initiate simultaneously fusions of two

symmetrically located cells and let both cells fuse completely. After both fusions are accomplished, one of the cells close to the tissue center is divided again.

The tissue shape during the whole simulation is quite regular and does not exhibit significant tissue bending. This is due to two factors—the time at which the processes are initiated and the position of proliferating or fusing cells. The experiment begins with proliferation of the middle cell and growth of its two daughter cells. This is similar to the tissue development shown in Fig. 7. However, here both cell fusions are initiated when the tissue shape is still horizontal. Therefore, in contrast to the simulation presented in Fig. 7, this tissue does not enter into the phase of bending. The timing and position of the fusing cells chosen here result in the regular shape of the tissue. Moreover, the new single cell proliferation is started in such a way to avoid another tissue bending. If one of the previously growing cells was chosen to proliferate again, then the tissue would bend inward as in Fig. 12. The growth of two new daughter cells in our simulation results only in the increase of already existing curvature of the tissue. It does not produce deep inward bending like in Fig. 7, because the shape of the tissue and the distribution of the opposite connections in the CT cells and the syncytium in both cases are different.

While this last experiment gives us evidence that our model can support development of tissue of regular shape, we do not claim that the presented ratio and order of cell processes constitutes any general rule for regularity of the trophoblast tissue. We have established that tissue development depends on the spatial and temporal distributions of cell proliferation and fusion.

4.3. ***Inward and outward tissue bending.*** We present here two simulations which lead to the fast tissue growth and result in inward or outward tissue bending. In both cases, all cell processes are executed symmetrically about the middle cell in the tissue. We expect that if cell processes are initiated symmetrically, then the shape of the tissue should remain symmetrical during its whole evolution. Moreover, such symmetrical tissue development does not bias interpretation of the obtained results.

Figure 12 shows a sequence from a simulation of several consecutive cell proliferations operating on a small part of the trophoblast tissue. At the beginning of this process the middle cell is divided. After it reaches maturity, its two new daughter cells are simultaneously divided again. Now the four daughter cells are growing, which produces the deep inward tissue bending or invagination.

The second numerical simulation presented in Fig. 13 shows the case of a deep outward tissue bending. This is a result of several consecutive cell proliferations operating on a small part of the trophoblast tissue initiated after the completion of a single cell fusion. This cell fusion leaves the trophoblast tissue in an almost flat horizontal shape with two middle cells only slightly shifted toward the tissue center. These two middle cells are then simultaneously divided and growth of their daughter cells results in tissue outward bending. This outward tissue bending is a positive feature from the biological and medical points of view, because it indicates

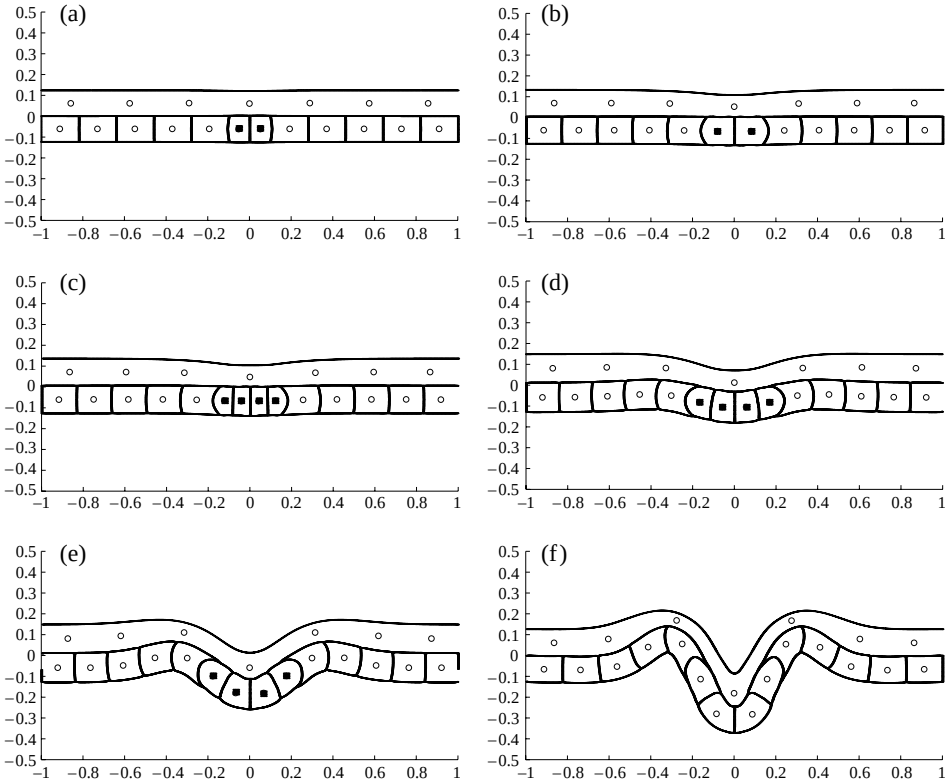

Figure 12. Simulations of the development of the trophoblast tissue resulting in a deep inward bending (invagination); shown at times (a) $t = 2.5$ s; (b) $t = 10$ s; (c) $t = 12.5$ s; (d) $t = 17.5$ s; (e) $t = 20$ s; (f) $t = 25$ s. Black squares at cell nuclei indicate which cells are currently fusing or proliferating.

a place when the chorionic villous tree starts to branch. For this reason this outward tissue bending is called budding.

These two numerical simulations show that cell proliferations lead to local tissue bending and that the direction of such bending depends on the previously completed processes and the way the tissue is shaped before the consecutive proliferations start to operate.

4.4. ***Simulations of trophoblast invaginations.*** Results of clinical research (Honore *et al.*, 1976; Novak *et al.*, 1988; Silvestre *et al.*, 1996; Lewis and Perrin, 1999; Kliman and French, 2001; Kliman *et al.*, 2001; Kliman and Segel, 2003) show that there is a connection between appearance of the deep trophoblast invaginations and genetic or developmental defects in the placenta and fetus. In this section we present results of numerical simulations which result in such deep inward tissue bending.

Figure 14 shows a sequence from a simulation of several consecutive cell proliferations operating on a small part of the trophoblast tissue. At the beginning of this process the middle cell is divided and their two daughter cells grow and

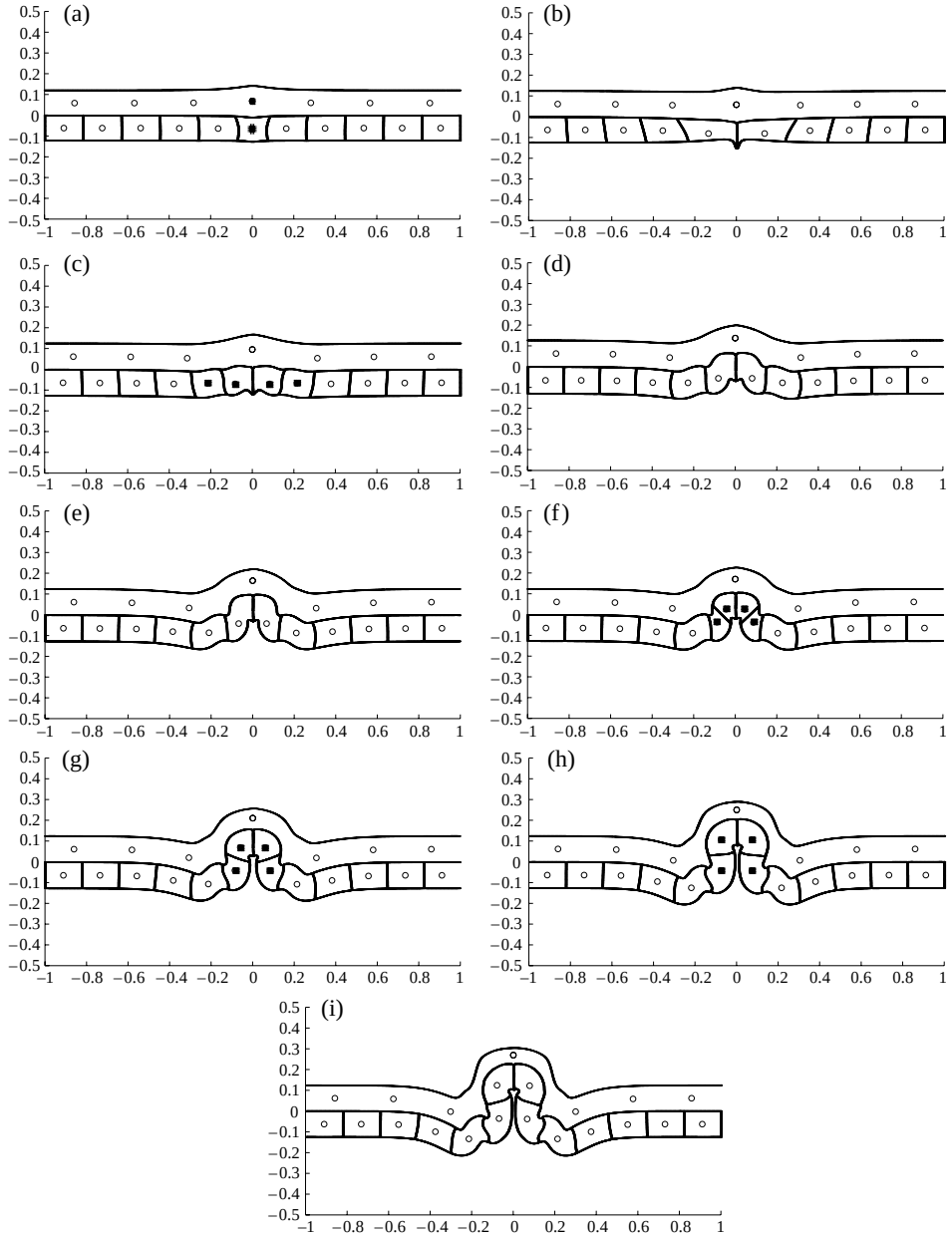

Figure 13. Simulations of the development of the trophoblast tissue resulting in a deep outward bending (budding); shown at times (a) $t = 6$ s; (b) $t = 21.5$ s; (c) $t = 27.5$ s; (d) $t = 32.5$ s; (e) $t = 37.5$ s; (f) $t = 40$ s; (g) $t = 45$ s; (h) $t = 50$ s; (i) $t = 60$ s. Black squares at cell nuclei indicate which cells are currently fusing or proliferating.

reach maturity. Once the CT cells reach the size of their common predecessor they are divided again simultaneously. When the process of proliferation of all four daughter cells is completed, two new cell divisions are initiated consecutively.

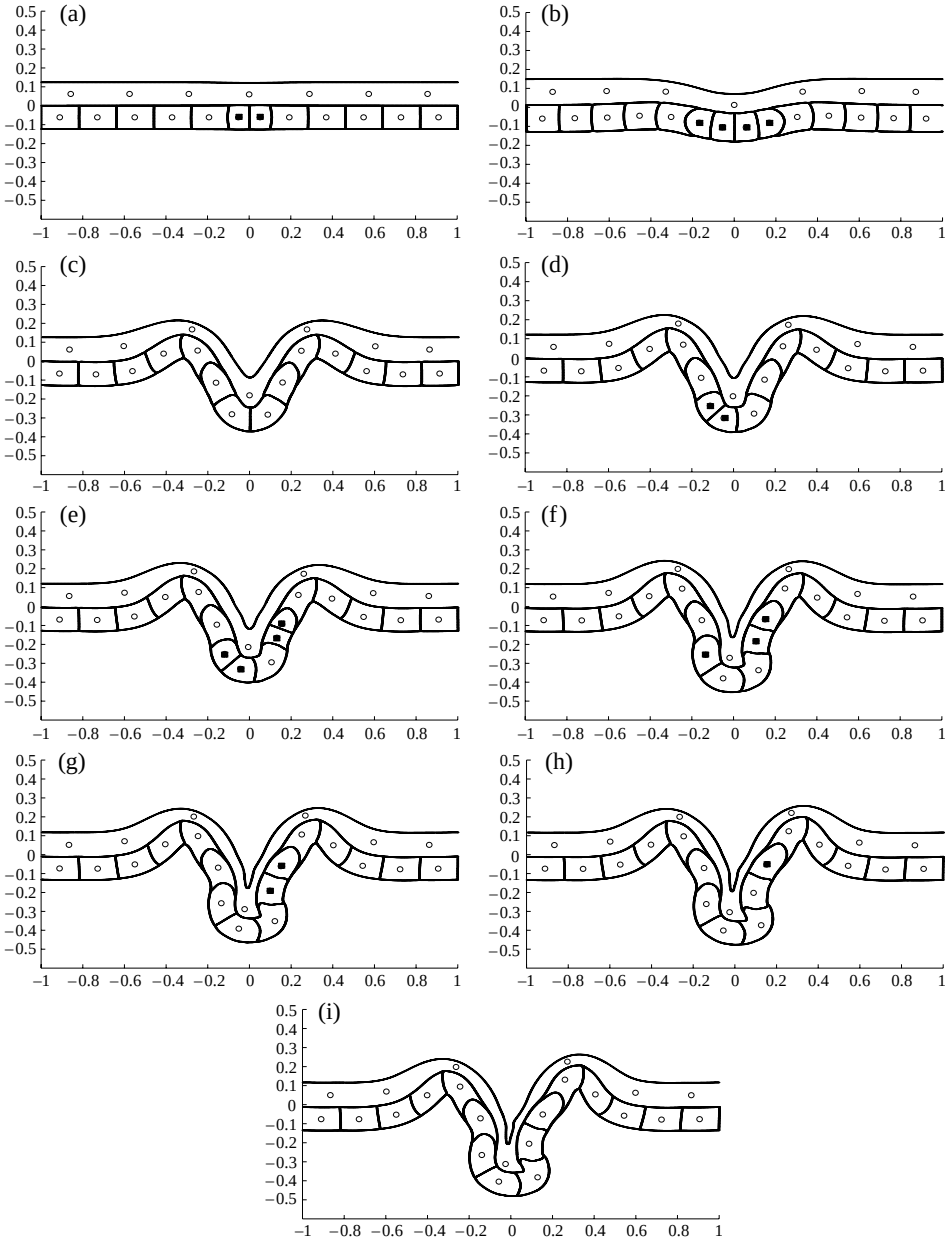

Figure 14. Simulation of the development of the trophoblast tissue resulting in the tissue invagination; shown at times (a) $t = 2.5$ s; (b) $t = 17.5$ s; (c) $t = 25$ s; (d) $t = 33$ s; (e) $t = 35$ s; (f) $t = 41$ s; (g) $t = 43$ s; (h) $t = 46$ s; (i) $t = 50$ s. Black squares at cell nuclei indicate which cells are currently fusing or proliferating.

These consecutive processes of cell proliferation result in the deep inward tissue bending which exhibits the similar shape to the tissue invaginations observed clinically (Kliman and French, 2001; Kliman and Segel, 2003).

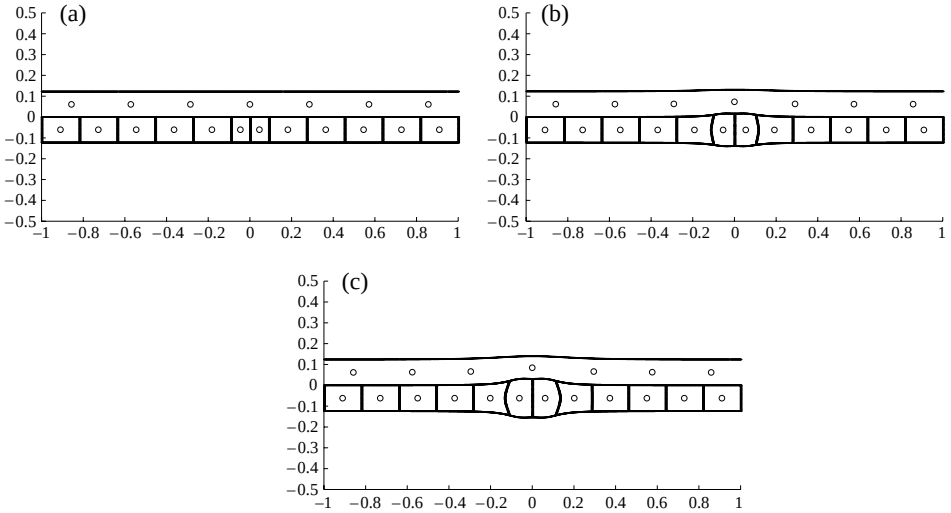

Figure 15. Simulation of the development of the trophoblast bilayer at times: (a) $t = 0.5$ s; (b) $t = 6$ s; (c) $t = 12$ s, in the case when there is no opposite connections in the CT cells and the stiffness constants are given by: $\mathcal{S}^{\mathrm{CT}}_{\mathrm{opp}} = \mathcal{S}^{\mathrm{ST}}_{\mathrm{opp}} = 0$ g s^{-2}, $\mathcal{S}^{\mathrm{CT}}_{\mathrm{adj}} = 0.1$ g s^{-2}, $\mathcal{S}^{\mathrm{ST}}_{\mathrm{adj}} = \mathcal{S}^{\mathrm{CT}}_{\mathrm{adj}}/25$, $\mathcal{S}^{\mathrm{BM}}_{\mathrm{adj}} = 10\mathcal{S}^{\mathrm{CT}}_{\mathrm{adj}}$.

5. Simulations of Different Viscoelastic Properties of Tissue Components

The three main components of the trophoblast tissue—the basement membrane, cytotrophoblastic cells and syncytium—have very different viscoelastic properties. The ST layer is the most flexible of the three, whereas the basement membrane is the most rigid. Because we model these three elements as collections of points connected by adjacent and opposite springs, we can capture different properties of each of them by adjusting spring stiffnesses. In this section we present several illustrative simulations of cell proliferation for different proportions between spring stiffnesses of the cytotrophoblastic cells (Section 5.1), the syncytium (Section 5.2) and the basement membrane (Section 5.3). We also discuss how the change of the springs stiffness affects behavior and development of the whole tissue.

5.1. ***Opposite connections in the cytotrophoblast.*** In the numerical simulations presented here the value of spring stiffness in the CT is varied, but proportions between spring stiffness in the CT cells, syncytium and basement membrane are preserved (cf. Table 1). All simulations show how the trophoblast tissue is developing during a single proliferation of the CT cell located in the middle of the tissue. Each simulation is completed when the tissue stabilizes its shape and the fluid field initiated by the movement of growing cells vanishes.

Figure 15 shows a sequence from simulation in which there are no opposite connections in the CT cells $\mathcal{S}^{\mathrm{CT}}_{\mathrm{opp}} = 0$ g s^{-2} and the adjacent connections in the CT cells

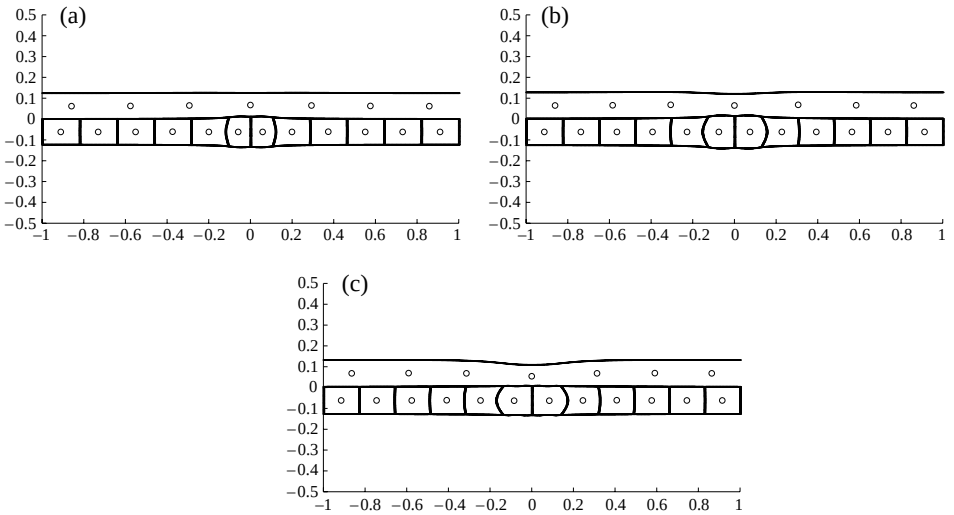

Figure 16. Simulation of the development of the trophoblast bilayer at times: (a) $t = 6$ s; (b) $t = 12$ s; (c) $t = 20$ s, in the case of small opposite connections in the CT cells. The stiffness constants are given by: $\mathcal{S}^{\mathrm{CT}}_{\mathrm{opp}} = \mathcal{S}^{\mathrm{CT}}_{\mathrm{adj}} = 0.01$ g s^{-2}, $\mathcal{S}^{\mathrm{ST}}_{\mathrm{opp}} = \mathcal{S}^{ST}_{\mathrm{adj}} = \mathcal{S}^{\mathrm{CT}}_{\mathrm{adj}}/25$, $\mathcal{S}^{\mathrm{BM}}_{\mathrm{adj}} = 10\mathcal{S}^{\mathrm{CT}}_{\mathrm{adj}}$.

have a spring stiffness of $\mathcal{S}^{\mathrm{CT}}_{\mathrm{adj}} = 0.1$ g s^{-2}. All springs in the ST layer (adjacent and opposite) have stiffness 25 times smaller than those in the CT layer and all adjacent springs in the basement membrane are 10 times stiffer than the adjacent connections in the CT cells.

Because CT cells have no opposite connections, their shapes are governed only by springs attached to adjacent boundary points. The sources of fluid put in the centers of two daughter cells cause the fluid to move uniformly in all directions away from the sources. Because the cells are tightly packed in the tissue, they offer resistance once the fluid flow pushes the boundaries of the growing cell against them. Therefore the fluid can move freely only in the directions not bounded by the neighboring cells, i.e., toward the syncytium and the basement membrane, which results in vertical ballooning.

In the second simulation presented here all CT cells have opposite connections with a small stiffness constant $\mathcal{S}^{\mathrm{CT}}_{\mathrm{opp}} = 0.01$ g s^{-2}. The adjacent connections in the CT cells have the same stiffness as the opposite ones, i.e., $\mathcal{S}^{\mathrm{CT}}_{\mathrm{adj}} = \mathcal{S}^{\mathrm{CT}}_{\mathrm{opp}} = 0.01$ g s^{-2}. All springs in the ST layer (adjacent and opposite) have stiffness 25 times smaller than those in the CT layer and all adjacent springs in the basement membrane are 10 times stiffer than the adjacent connections in the CT cells. Figure 16 shows a few snapshots from this simulation. It can be seen that the tissue has a small tendency to vertical ballooning at the beginning of its development, but it is reduced shortly by the existing opposite connections in the CT cells. The shape of the tissue stabilizes in the horizontal straight line and never reaches the phase of bending.

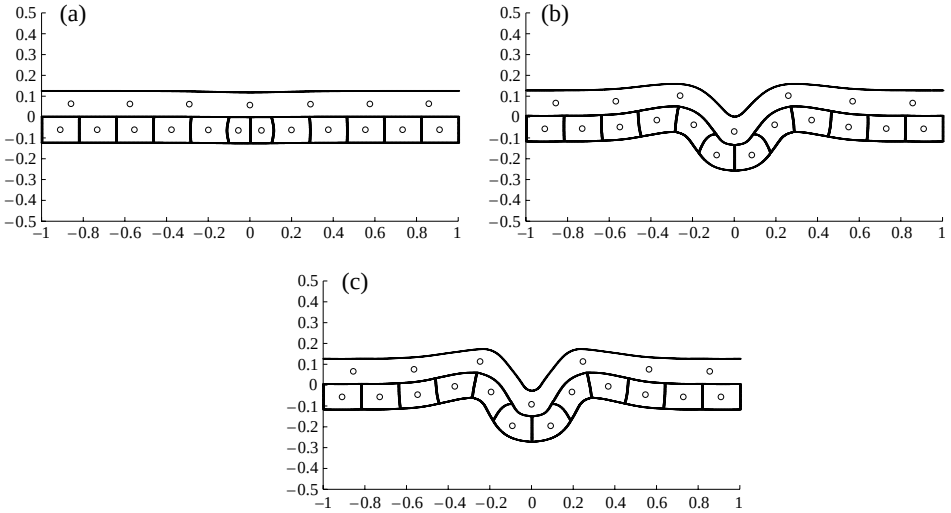

Figure 17. Simulation of the development of the trophoblast bilayer at times: (a) $t = 3$ s; (b) $t = 10$ s; (c) $t = 18$ s, in the case of large opposite connections in the CT cells. The stiffness constants are given by: $\mathcal{S}^{\mathrm{CT}}_{\mathrm{opp}} = \mathcal{S}^{\mathrm{CT}}_{\mathrm{adj}} = 1$ g s^{-2}, $\mathcal{S}^{ST}_{\mathrm{opp}} = \mathcal{S}^{ST}_{\mathrm{adj}} = \mathcal{S}^{\mathrm{CT}}_{\mathrm{opp}}/25$, $\mathcal{S}^{BM}_{\mathrm{adj}} = 10\mathcal{S}^{\mathrm{CT}}_{\mathrm{opp}}$.

In the last simulation all CT cells have opposite and adjacent connections with large spring stiffness $\mathcal{S}^{\mathrm{CT}}_{\mathrm{opp}} = \mathcal{S}^{\mathrm{CT}}_{\mathrm{adj}} = 1$ g s^{-2}. All springs in the ST layer (adjacent and opposite) have stiffness 25 times smaller than those in the CT layer and all adjacent springs in the basement membrane are 10 times stiffer than the adjacent connections in the CT cells. A few snapshots from this simulation are shown in Fig. 17. In this case the tissue starts bending downward very early and the impact of the opposite connections is very intense. The shape of the tissue stabilizes and exhibits a deep inward bending.

The trophoblast tissue in these three numerical simulations exhibits a quite different behavior—a vertical ballooning of two growing cells only when there are no opposite connections, a regular horizontal tissue shape in the case of small opposite connections and deep inward bending when the opposite connections have large stiffness. In all three simulations the proportions in spring stiffnesses between the basement membrane, the ST and CT layers are preserved and only the value of the stiffness of the opposite connections in the CT layer is varied. Therefore, different viscoelastic properties of the CT layer lead to different behavior of the whole trophoblast tissue.

5.2. ***Opposite connections in the syncytiotrophoblast.*** In the simulations presented in this section the value of spring stiffness in the ST is varied. All simulations show how the trophoblast tissue is developing during a single proliferation of the cell located in the middle of the CT. Each simulation is completed when the

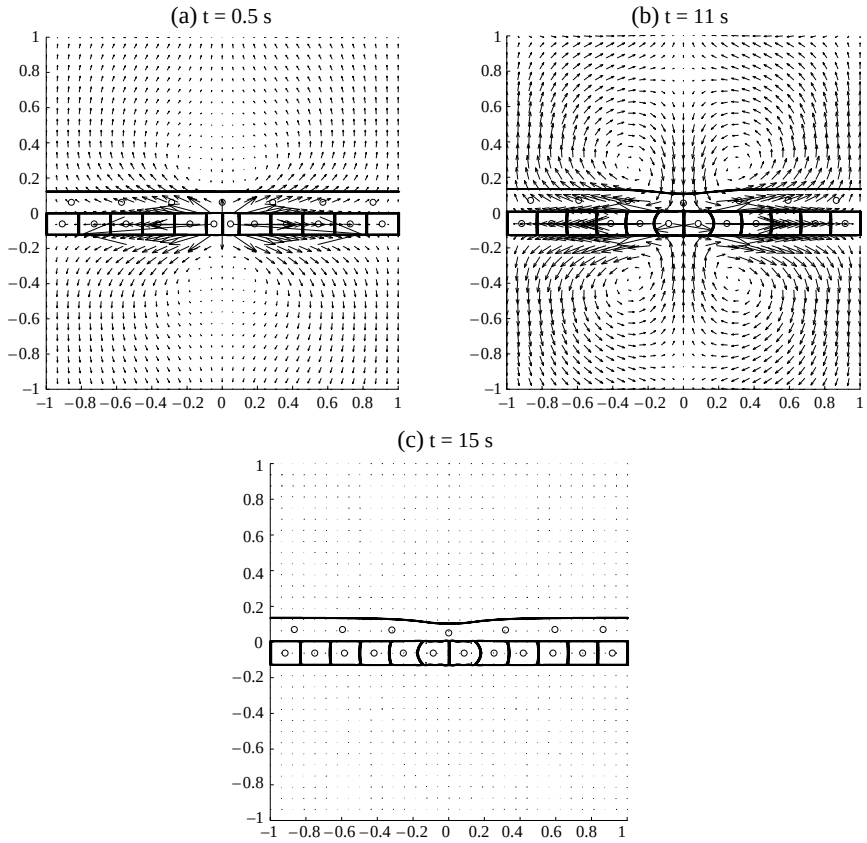

Figure 18. Simulation of the development of the trophoblast bilayer in the case when there are no opposite connections in the ST layer and moderate connections in the CT cells. $\mathcal{S}^{\mathrm{CT}}_{\mathrm{opp}} = \mathcal{S}^{\mathrm{CT}}_{\mathrm{adj}} = 0.1\ \mathrm{g\ s^{-2}}$, $\mathcal{S}^{\mathrm{ST}}_{\mathrm{opp}} = 0\ \mathrm{g\ s^{-2}}$, $\mathcal{S}^{\mathrm{ST}}_{\mathrm{adj}} = \mathcal{S}^{\mathrm{CT}}_{\mathrm{opp}}/25$, $\mathcal{S}^{BM}_{\mathrm{adj}} = 10\mathcal{S}^{\mathrm{CT}}_{\mathrm{opp}}$.

tissue stabilizes its shape and the fluid field initiated by the movement of growing cells vanishes.

Figure 18 shows a sequence from simulation in which there are no opposite connections in the ST layer, $\mathcal{S}^{ST}_{\mathrm{opp}} = 0\ \mathrm{g\ s^{-2}}$. The adjacent and opposite connections in the CT cells have a spring stiffness of $\mathcal{S}^{\mathrm{CT}}_{\mathrm{opp}} = \mathcal{S}^{\mathrm{CT}}_{\mathrm{adj}} = 0.1\ \mathrm{g\ s^{-2}}$. The adjacent springs in the ST layer have stiffness 25 times smaller than those in the CT layer and all adjacent springs in the basement membrane are 10 times stiffer than the adjacent connections in the CT cells. The fluid around the growing cells is moving horizontally due to the operating opposite connections inside the CT cells. The flow pattern is symmetrical because there is no resistance from the syncytium due to the lack of the opposite connections in the ST layer. This horizontal, symmetrical flow pattern remains almost unchanged as long as the sources are active and the tissue finally stabilizes to a horizontal shape.

In the second simulation presented here there are still no opposite connections in the ST layer, $\mathcal{S}^{ST}_{\mathrm{opp}} = 0\ \mathrm{g\ s^{-2}}$, but this case differs from the previous one in the value

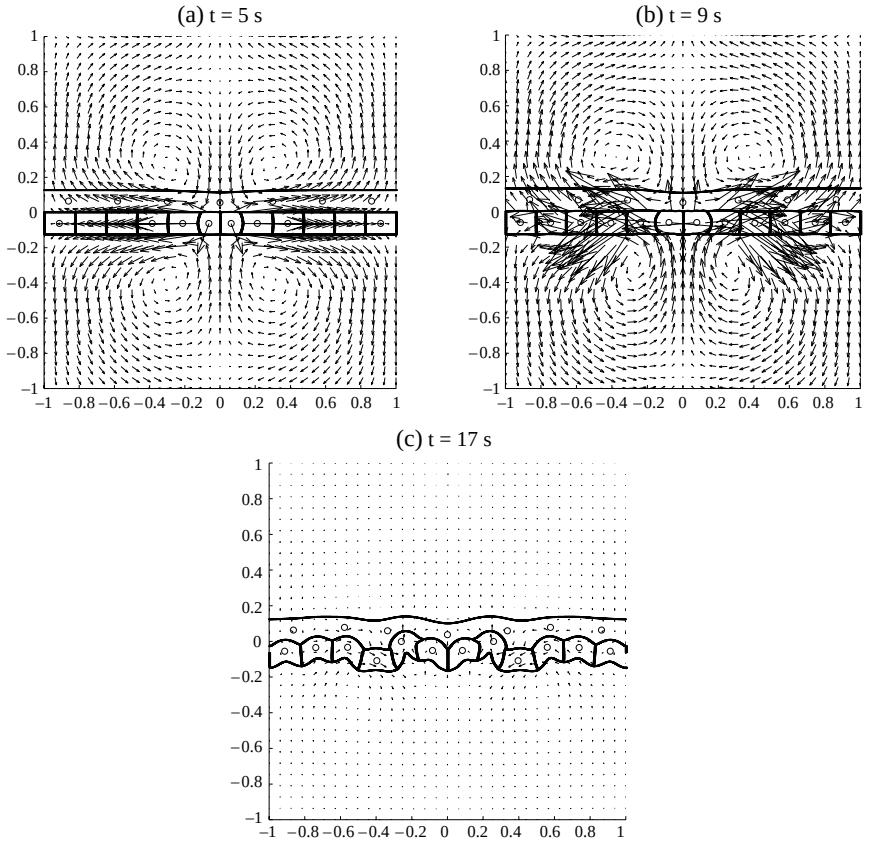

Figure 19. Simulation of the development of the trophoblast bilayer in the case when there are no opposite connections in the ST layer and large connections in the CT cells. $\mathcal{S}^{\mathrm{CT}}_{\mathrm{opp}} = \mathcal{S}^{\mathrm{CT}}_{\mathrm{adj}} = 1\ \mathrm{g\ s}^{-2}$, $\mathcal{S}^{\mathrm{ST}}_{\mathrm{opp}} = 0\ \mathrm{g\ s}^{-2}$, $\mathcal{S}^{\mathrm{ST}}_{\mathrm{adj}} = \mathcal{S}^{\mathrm{CT}}_{\mathrm{opp}}/25$, $\mathcal{S}^{\mathrm{BM}}_{\mathrm{adj}} = 10\mathcal{S}^{\mathrm{CT}}_{\mathrm{opp}}$.

of stiffness of the connections in the cytotrophoblastic cells. Here the adjacent and opposite connections in the CT layer are very large $\mathcal{S}^{\mathrm{CT}}_{\mathrm{opp}} = \mathcal{S}^{\mathrm{CT}}_{\mathrm{adj}} = 1\ \mathrm{g\ s}^{-2}$. The adjacent springs in the ST layer have stiffness 25 times smaller than those in the CT layer and all adjacent springs in the basement membrane are 10 times stiffer than the adjacent connections in the CT cells. Figure 19 shows a few snapshots from this simulation. Initially the fluid flow around the tissue is horizontal. However, when the growing cells almost double their area, the large opposite connections inside them greatly influence motion of the fluid. Finally the tissue achieves the shape with no explicit bending. Moreover, the cells are packed in such a way, which may still be considered a horizontal layer.

In the last simulation, the opposite and adjacent connections in both layers have the same large stiffness $\mathcal{S}^{ST}_{\mathrm{opp}} = \mathcal{S}^{\mathrm{CT}}_{\mathrm{opp}} = \mathcal{S}^{ST}_{\mathrm{adj}} = \mathcal{S}^{\mathrm{CT}}_{\mathrm{adj}} = 1\ \mathrm{g\ s}^{-2}$. All adjacent springs in the basement membrane are 10 times stiffer than the adjacent connections in the CT cells. A few stages of tissue development in this case are shown in Fig. 20.

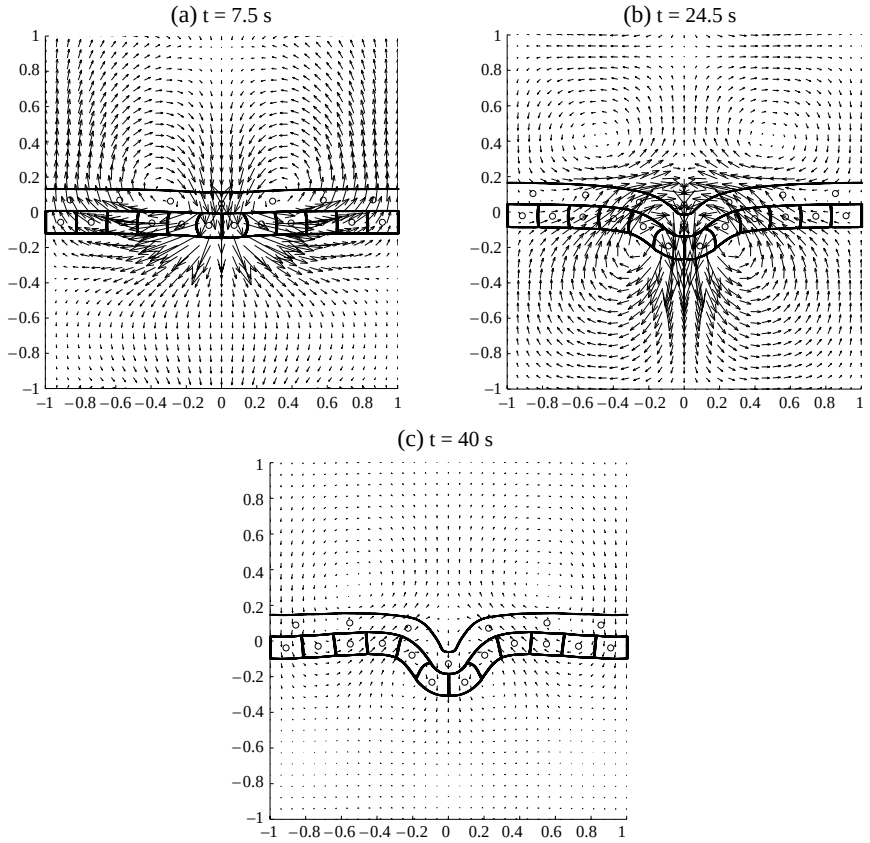

Figure 20. Simulation of the development of the trophoblast bilayer in the case when the opposite and adjacent connections in the ST and CT layers are equal. $\mathcal{S}^{\mathrm{CT}}_{\mathrm{opp}} = \mathcal{S}^{\mathrm{CT}}_{\mathrm{adj}} = \mathcal{S}^{\mathrm{ST}}_{\mathrm{opp}} = \mathcal{S}^{ST}_{\mathrm{adj}} = 1\ \mathrm{g\ s}^{-2}$, $\mathcal{S}^{BM}_{\mathrm{adj}} = 10\mathcal{S}^{\mathrm{CT}}_{\mathrm{opp}}$.

Because the large opposite connections are present in both layers, the final shape of the tissue exhibits an inward bending.

The trophoblast tissue in these three numerical simulations exhibits a quite different behavior—a flat horizontal shape of the tissue when there are no opposite connections in the syncytium and moderate opposite connection in the CT cells, a horizontal layer of squeezed CT cells in the case of absent opposite connections in the ST layer and large opposite connections in the CT and deep inward bending when the opposite connections in both layers have equal large stiffnesses. Therefore, different viscoelastic properties of the ST layer lead to different behavior of the whole trophoblast tissue.

5.3. ***Adjacent connections in the basement membrane.*** We present here results of three numerical simulations in which the value of spring stiffness of the adjacent connections of the basement membrane is varied. Because the basement membrane

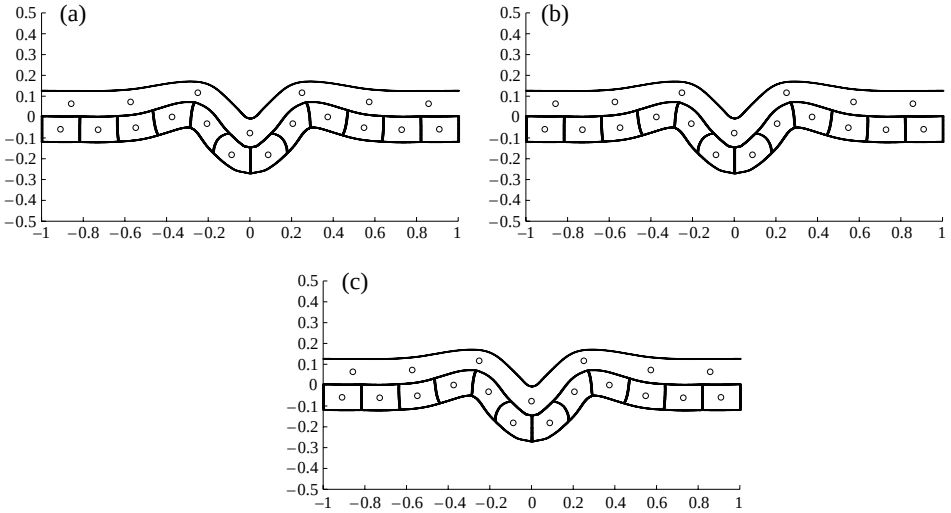

Figure 21. Simulation of the development of the trophoblast tissue for different spring connections of the basement membrane. The stiffness constants are given by: $\mathcal{S}^{\mathrm{CT}}_{\mathrm{opp}} = \mathcal{S}^{\mathrm{CT}}_{\mathrm{adj}} = 0.1$ g s^{-2}, $\mathcal{S}^{ST}_{\mathrm{opp}} = \mathcal{S}^{ST}_{\mathrm{adj}} = \mathcal{S}^{\mathrm{CT}}_{\mathrm{opp}}/25$ and (a) $\mathcal{S}^{BM}_{\mathrm{adj}} = 10\mathcal{S}^{\mathrm{CT}}_{\mathrm{adj}}$; (b) $\mathcal{S}^{BM}_{\mathrm{adj}} = 10^3\mathcal{S}^{\mathrm{CT}}_{\mathrm{adj}}$; (c) $\mathcal{S}^{BM}_{\mathrm{adj}} = 10^5\mathcal{S}^{\mathrm{CT}}_{\mathrm{adj}}$.

is the most rigid of all components of the trophoblast tissue, its spring connections are set up to have a larger value than those in the CT cells and the ST layer.

In the presented simulations the adjacent springs of the basement membrane are 10, 10^3 and 10^5 times greater then that in the CT cells. All simulations show how the trophoblast tissue is developing during a proliferation of a single cell located at the middle of the CT layer. Each simulation is completed when the tissue stabilizes its shape. The final shape of the tissue in all three cases is shown in Fig. 21. These simulations show no significant difference in the shape and behavior of the growing tissue in all cases considered.

6. DISCUSSION

We have presented a computational model based on the immersed boundary method for studying the mechanics of growth of a trophoblast bilayer. This model allows us to capture elastic properties of the cells, as well as the mechanics of the viscous, incompressible fluid in which they sit. It also takes into account the differences in the structure of each layer of the tissue—the mononuclear cytotrophoblasts and the multinucleated syncytiotrophoblast and models them accordingly. The representation of the cytotrophoblast includes a detailed description of the structure of a single cell and a mechanism that allows single cells to form one continuous tissue layer. All cells act together, even though each of them is modeled as a

separate object. The representation of the multinucleated ST enables smooth and continuous covering of the underlying CT layer, despite its shape, which can vary during the development of the tissue.

We have incorporated in our model three cell processes—division, growth and fusion—which play a crucial role in the development of the whole placenta. Computational results presented in Sections 3.1 and 3.2 demonstrate the ability of our model to simulate the behavior of a proliferating, growing or fusing cell which has been observed in biological and clinical research (Boyd and Hamilton, 1970; Kliman *et al*., 1986, 1987; Alberts *et al*., 1994; Benirschke and Kaufmann, 1995). In addition, our model includes a simple form of cell communication allowing temporal and spatial control of the initiation of cell processes. In general, cell processes operate on cells chosen arbitrarily from those which constitute the CT, but we have employed a mechanism of checking whether the chosen cell may undergo the given process. This control mechanism can be summarized as follows. The already fusing cell cannot be chosen to fuse again. A fusing cell may not start proliferating, because cell fusion is accompanied by changes in the cell nucleus that causes it to lose its mitotic activity. A growing cell cannot be chosen to proliferate again, because a cell must reach maturity before it starts the next division. A cell can fuse at any moment of its life. Such communication prevents conflicts between operating cell processes.

The computational results presented in Section 4 demonstrate the ability of our model to capture the behavior of the whole living tissue whereas the initiation and operation of all cell processes are limited to single cells only. Moreover, our model is capable of capturing more complex phenomena, like outward and inward tissue bending, which have been observed clinically in the trophoblast tissue of normal and abnormal placentas (Kliman and French, 2001; Kliman *et al*., 2001). We illustrate this qualitative agreement of our computational model with clinical observations of both abnormal and normal placentas. The results of computer simulations were accomplished by suitable choices of temporal and spatial distributions of proliferating and fusing cells.

The first example is presented in Fig. 22. A bilayer trophoblast tissue in this case does not exhibit regular and smooth covering of the villous core, but shows deep inward bending. In the accompanying computer simulation such an effect was obtained by initiating several consecutive proliferations of cells occupying the same small area of the tissue. Other computer simulations of inward tissue bending were discussed in Sections 4.3 and 4.4. The depth of the numerically obtained invagination depends on the number and location of cells which have proliferated. The deepest inward bending can be achieved when the new born cells undergo cell division right after they reach maturity, i.e., when several generations of cells cooperate in the formation of the trophoblast invagination.

The second example (Fig. 23) shows a section of the trophoblast tissue in which several invaginations are located close to each other. We have modeled such tissue scalloping by alternating proliferations and fusions of a few cells occupying

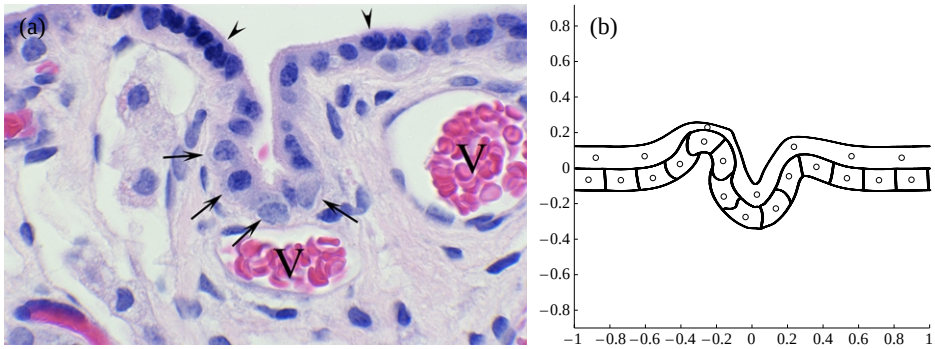

Figure 22. Comparison of *in vivo* (a) and computer simulated (b) trophoblast invagination. (a) Representative region of trophoblast invagination. Note increased density of CTs (arrows) at base of invagination. Syncytial trophoblast layer (arrow heads). Vessels containing fetal erythrocytes (V). (b) Computer simulation invagination obtained by numerous proliferations of cells located close to the base of invagination.

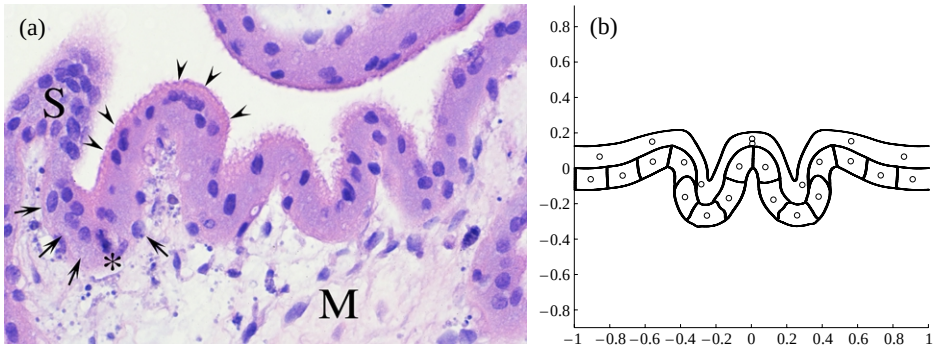

Figure 23. Comparison of *in vivo* (a) and computer simulated (b) scalloping trophoblast. (a) Region of scalloping in a first-trimester villous. Note increased density of CTs at base of invagination (arrows) and increased numbers of ST nuclei in regions of evaginations (arrow heads and S). As shown in Fig. 1, mitotic figures within the CT layer are common ($*$). Villous matrix core (M). (b) Computer simulation of scalloped trophoblast bilayer obtained by alternating proliferations and fusions of a few cells occupying a common area of the tissue.

a small common area of the tissue. Two inward bendings in our simulation were obtained as an effect of cell proliferations in the very same way as the single invagination described in the previous example. The outward bending located in between two invaginations is a result of cell fusion. The depth of inward and outward tissue bends in our simulation depends strongly on the number of cells which have proliferated.

The final example, presented in Fig. 24, shows a micrograph picture of a section of the trophoblast tissue which bends outward forming an evagination. This kind of bending, in contrast to the two previous examples, occurs in the normal

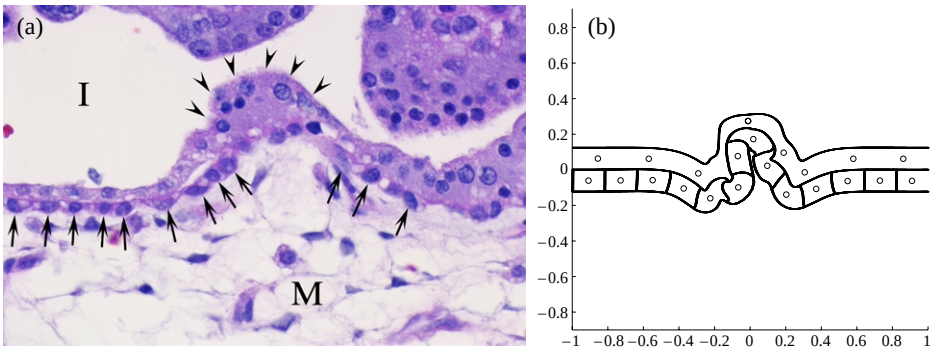

Figure 24. Comparison of *in vivo* (a) and computer simulated (b) trophoblast evagination. (a) Region of budding (evagination) seen in a first trimester villous. Note continuous layer of CTs in regions on either side of evagination (arrows) and increased amount of cytoplasm and number of nuclei in ST layer in region of evagination (arrow heads). Villous matrix core (M) and intervillous space containing a few maternal erythrocytes (I). (b) Computer simulation of evagination obtained by initiating several cell fusions followed by consecutive proliferations of cells occupying the same small area of the tissue.

placenta and can indicate the place where the chorionic villous tree starts to branch. In the presented simulation, such an effect was obtained by initiating several cell fusions followed by consecutive proliferations of cells occupying the same small area of the tissue. The growth of each daughter cell results in the bending of the whole tissue and its outward direction is caused by the preceding cell fusion. Another computer simulation of a tissue evagination was discussed in Section 4.3.

In Section 5 we demonstrated the mechanical effects of stiffness strengths in both layers of trophoblast tissue and showed how these affect the shape of the cytotrophoblastic cells and the whole tissue. Lack of opposite connections in the syncytium or their very small stiffness leads to a regular horizontal tissue shape, despite the stiffness of the opposite connections in the CTs. When the opposite connections are present in the ST layer, the whole tissue bends. Moreover, in the case of equal stiffness of opposite springs in both trophoblast layers, the process of cell proliferation creates a deep downward bending. Note that both tissue layers are filled with the fluid of the same viscosity; thus changing the stiffness of the opposite connections in a particular layer results in changing its viscoelastic properties. To our knowledge, the problem of resistance offered by the syncytium or the mother's blood was not considered in any clinical or experimental investigation. Therefore, we do not have any experimental evidence to support the findings suggested by our model. However, the problem of how mechanical tension influences cell form and function was studied in numerous kinds of eukaryotic cells [for review see Chicurel *et al.* (1998), Van Essen (1997)]. It was also shown in Davidson *et al.* (1995) that the primary invagination of the vegetal plate in the sea urchin during the process of gastrulation is a consequence of the pattern of forces exerted by cells and by the extracellular matrix.

The computational model presented in this paper constitutes a promising starting point for studying the mechanics of the trophoblast tissue growth and other biological phenomena discussed above. Some improvements of this model are currently being developed. We are in the process of modifying the mechanism of cell fusion to allow not only confluence of the cytoplasms of syncytium and the fusing cell, but also aggregation of two cytotrophoblastic cells. This will enable us to model a complete process of branching of the chorionic villous tree. A quantitative analysis of the relation between tissue bending and frequencies of fusing and proliferating cells, as well as their spatial and temporal distributions, is also a subject of our investigation. Moreover, we are currently working on a three-dimensional model of the trophoblast tissue, which will enable us to investigate the formation of tissue invaginations in diverse planes and cross-sections of the chorionic villous tree. This in turn will allow us to observe the formation and development of trophoblast inclusions, i.e., islands of trophoblasts located within the villous core.

Additional materials. The animations of cell processes discussed in this paper as well as several simulations of the developing trophoblast tissues, (including the phenomena of tissue evaginations and invaginations) have been converted to QuickTime™ and audio/video *AVI* movies and posted on the World Wide Web at the following location:

`http://www.math.tulane.edu/~rejniak/trophoblast.html`.

ACKNOWLEDGEMENTS

The work of L Fauci was supported by the National Science Foundation Grants DMS-9805492 and DMS-0201063. The work of K Rejniak was supported in part by DMS-9805492 and by NSF under agreement no. 0112050. Computations were performed at the Center for Computational Science at Tulane and Xavier Universities, supported by the US Department of Energy contract DE-FG02-01ER63119.

REFERENCES

Alberts, B., D. Bray, J. Lewis, M. Raff, K. Roberts and J. D. Watson (1994). *Molecular Biology of the Cell*, Garland Publishing.

Arthurs, K. M., L. C. Moore, C. S. Peskin, E. B. Pitman and H. E. Layton (1998). Modeling arteriolar flow and mass transport using the immersed boundary method. *J. Comput. Phys.* **147**, 402–440.

Batchelor, G. K. (1967). *An Introduction to Fluid Dynamics*, Cambridge Press.

Benirschke, K. and P. Kaufmann (1995). *Pathology of the Human Placenta*, Springer.

Bottino, D. C. (1998). Modeling viscoelastic networks and cell deformation in the context of the immersed boundary method. *J. Comput. Phys.* **147**, 86–113.

Bottino, D. C. and L. J. Fauci (1998). A computational model of ameboid deformation and locomotion. *Eur. Biophys. J.* **27**, 532–539.

Boyd, J. D. and W. J. Hamilton (1970). *The Human Placenta*, Cambridge: W. Heffer & Sons, Ltd.

Chicurel, M. E., Ch. S. Chen and D. E. Ingber (1998). Cellular control lies in the balance of forces. *Curr. Opin. Cell Biol.* **10**, 232–239.

Cortez, R. and M. Minion (2000). The Blob projection method for the immersed boundary problems. *J. Comput. Phys.* **161**, 428–453.

Davidson, L. A., M. A. R. Koehl, R. Keller and G. F. Oster (1995). How do see urchins invaginate? Using biomechanics to distinguish between mechanisms of primary invagination. *Development* **121**, 2005–2018.

Dillon, R. H. and L. J. Fauci (2001). A fluid-structure interaction model of ciliary beating, in *Computational Modeling in Biological Fluid Dynamics*, The IMA Volumes in Mathematics and its Applications **124**, L. J. Fauci and S. Gueron (Eds), Springer, pp. 71–80.

Dillon, R. and L. Fauci (2000a). A microscale model of bacterial and biofilm dynamics in porus media. *Biotechnol. Bioeng.* **68**, 536–547.

Dillon, R. and L. Fauci (2000b). An integrative model of internal axoneme mechanics and external fluid dynamics in ciliary beating. *J. Theor. Biol.* **207**, 415–430.

Dillon, R., L. J. Fauci, A. Fogelson and D. Gaver (1996). Modeling biofilm processes using the immersed boundary method. *J. Comput. Phys.* **129**, 57–73.

Dillon, R., L. J. Fauci and D. Gaver III (1995). Microscale model of bacterial swimming, chemotaxis and substrate transport. *J. Theor. Biol.* **177**, 325–340.

Dillon, R. and H. G. Othmer (1999). A mathematical model for outgrowth and spatial pattering of the vertebrate limb bud. *J. Theor. Biol.* **197**, 295–330.

Fauci, L. J. (1990). Interaction of oscillating filaments: a computational study. *J. Comput. Phys.* **86**, 294–313.

Fauci, L. J. and A. L. Fogelson (1993). *Truncated Newton Method and the Modeling of Complex Immersed Elastic Structures*. Communication on Pure and Applied Mathematics, **XLVI**, pp. 787–818.

Fauci, L. F. and C. S. Peskin (1988). A computational model of aquatic animal locomotion. *J. Comput. Phys.* **77**, 85–107.

Fogelson, A. L. (1984). A mathematical model and numerical method for studying platelet adhesion and aggregation during blood clotting. *J. Comput. Phys.* **56**, 111–134.

Honore, L. H., F. J. Dill and B. J. Poland (1976). Placental morphology in spontaneous human abortuses with normal and abnormal karyotypes. *Teratology* **14**, 151–166.

Jung, E. and C. S. Peskin (2001). 2-D simulations of valveless pumping using the immersed boundary method. *SIAM J. Sci. Comput.* **23**, 19–45.

Kliman, H. J. (1999). *Trophoblast to Human Placenta*, Encyclopedia of Reproduction **4**, E. Knobil and J. D. Neill (Eds), Academic Press.

Kliman, H. J., M. A. Feinman and J. F. Strauss III (1987). Differentiation of human cytotrophoblast into syncytiotrophoblast in culture. *Trophoblast Res.* **4**, 407–421.

Kliman, H. J. and L. French (2001). Trophoblast inclusions are associated with karyotypic abnormalities. *21st Annual Meeting of the Society for Maternal-Fetal Medicine*, Reno, NV.

Kliman, H. J., J. E. Nestler, E. Sermasi, J. M. Sanger and J. F. Strauss III (1986). Purification, characterization and in vitro differentiation of cytotrophoblasts from human term placentae. *Endocrinology* **118**, 1567–1582.

Kliman, H. J. and L. Segel (2003). The placenta may predict the baby. *J. Theor. Biol.* **225**, 143–145.

Kliman, H. J., L. Segel, L. Fauci and R. Cortez (2001). Model for the formation of trophoblast inclusions in chorionic villi. *21st Annual Meeting of the Society for Maternal-Fetal Medicine*, Reno, NV.

Lewis, S. H. and E. Perrin (1999). *Pathology of the Placenta*, Churchill Livingstone.

Mayhew, T. M. (2001). Villous trophoblast of human placenta: a coherent view of its turnover, repair and contribution to villous development and maturation. *Histol. Histopathol. Cell. Mol. Biol.* **16**, 1213–1224.

McQueen, D. M. and C. S. Peskin (1989). A three-dimensional computational method for blood flow in the heart. II. Contractible fibers. *J. Comput. Phys.* **82**, 289–297.

Novak, R., D. Agamanolis, S. Dasu, H. Igel, M. Platt, H. Robinson and B. Shehata (1998). Histologic analysis of placental tissue in first trimester abortions. *Pediatr. Pathol.* **8**, 477–482.

Peskin, C. S. (1972). Flow patterns around heart valves: a numerical method. *J. Comput. Phys.* **10**, 252–271.

Peskin, C. S. (1977). Numerical analysis of blood flow in the heart. *J. Comput. Phys.* **25**, 220–252.

Peskin, C. S. (2002). The immersed boundary method. *Acta Numerica*, 1–39.

Peskin, C. S. and D. M. McQueen (1995). A general method for computer simulation of biological systems interacting with fluids, in *Biological Fluid Dynamics*, vol. 19, C. P. Ellington and T. J. Pedley (Eds), Cambridge Press, pp. 265–276.

Peskin, C. S. and D. M. McQueen (1989). A three-dimensional computational method for blood flow in the heart. I. Immersed elastic fibers in a viscous incompressible fluid. *J. Comput. Phys.* **81**, 327–405.

Rejniak, K. A. (2002). A computational model of the mechanics of growth of a trophoblast tissue, PhD thesis, Tulane University, New Orleans, USA.

Silvestre, E., V. Cusi, M. Borras and J. Anitch (1996). Cytogenetic and morphologic findings in chorionic villi from spontaneous abortions. *Birth Defects; Original Article Series* **30**, 353–357.

Van Essen, D. C. (1997). A tension-based theory of morphogenesis and compact wiring in the central nervous system. *Nature* **285**, 313–318.

Received 29 April 2003 and accepted 26 June 2003